1969-06

Simulation of a liquid metal fast breeder reactor on a hybrid computer

Keller, Charles Lee

Monterey, California. Naval Postgraduate School

SIMULATION OF A LIQUID METAL FAST BREEDER REACTOR ON A HYBRID COMPUTER

by

Charles Lee Keller

United States
Naval Postgraduate School

THESIS

SIMULATION OF A LIQUID METAL

FAST BREEDER REACTOR ON A HYBRID COMPUTER

by

Charles Lee Keller

June 1969

Simulation of a Liquid Metal Fast Breeder Reactor on a Hybrid Computer

by

Charles Lee Keller
Lieutenant Commander, United States Coast Guard
B.S., United States Coast Guard Academy, 1960

Submitted in partial fulfillment of the
requirements for the degree of

MASTER OF SCIENCE IN PHYSICS

from the

NAVAL POSTGRADUATE SCHOOL
June 1969

ABSTRACT

A Liquid Metal Fast Breeder Reactor is simulated on a hybrid computer to study the transient behavior of the neutron density during a controlled reactivity input disturbance.

The nonlinear partial differential equations of heat flow are reduced by a discrete space-continuous time method to ordinary nonlinear differential equations which are readily solved on the analog computer. Use is made of time multiplexing of the analog circuitry in order to reduce the number of components. An open-loop iteration process is employed to solve the closed-loop feedback system.

Recently conducted research with the open-loop iteration method has demonstrated that a large number of iterations are required for convergence. An algorithm is developed which gives an improvement in the convergence rate for early values of time. For times greater than two seconds a stability problem with the converged solution was encountered and is discussed with some observations and comments.

Innovations are introduced in the simulation of the neutron kinetics equations and in the handling of the nonlinear thermal properties of the uranium oxide fuel.

TABLE OF CONTENTS

LIST OF TABLES

LIST OF ILLUSTRATIONS

TABLE OF SYMBOLS AND ABBREVIATIONS

Symbol	Definition	Units
A_{Dopp}	Doppler coefficient	Reactivity units
B_{exp}	Fuel expansion coefficient	Reactivity units/^{o}C
C_{cool}	Sodium void coefficient	Reactivity units/^{o}C
$c_i(t)$	Density of the i^{th} group of delayed neutron precursor	Number/cm^3
c(t)	Density of the assumed one precursor at time t	Number/cm^3
c(0)	Density of the assumed one precursor at time t = 0	Number/cm^3
c	Specific heat (subscript f refers to fuel, c to cladding and cool to coolant)	Watt-sec/cm^3-^{o}C
d	Density (subscript f refers to fuel, c to cladding, and cool to coolant)	Gm/cm^3
D(0)	Normalized precursor concentration at time t = 0	Pure number
D(t)	Normalized precursor concentration at time t	Pure number
G(t)	Mass flow rate of coolant	Gm/cm^2-sec
h	Heat transfer coefficient between cladding and coolant	Watts/cm^2-^{o}C
H	Heat flow rate across clad-coolant interface	Watts/cm^2
k_s	Analog scaling factor for power	Watts/cm^3-Volt
k_K	Analog scaling factor for thermal conductivity	Watts/cm-^{o}C-Volt
k_T	Analog scaling factor for temperature	^{o}K/Volt

Symbol	Definition	Units
k_N	Analog scaling factor for normalized neutron concentration	Pure number/Volt
K(T)	Thermal conductivity (subscript c refers to cladding and f to fuel)	Watts/cm-^{o}C
$K_{f,i+1,i}$	Thermal conductivity at boundary between node i and node i + 1	Watts/cm-^{o}C
K(t)	Reactivity (subscript Dopp refers to Doppler effect, exp to fuel expansion, and cool to coolant expansion	Dollars
K_f	Reactivity due to feedback	Dollars
K_e	Reactivity due to controlled disturbance	Dollars
ℓ	Prompt neutron lifetime	Sec
n(O)	Neutron density at time t = 0	Neutrons/cm^3
n(t)	Neutron density at time t	Neutrons/cm^3
N(O)	Normalized neutron density at time t = 0	Pure number
N(t)	Normalized neutron density at time t	Pure number
$Q(r,\theta,z,t)$	Power produced per unit volume by fission process within fuel	Watts/cm^3
r_i	Radius of node i	Cm
r	Radial variable within fuel pin	Cm
r_f	Radius of fuel	Cm
r_c	Outer radius of cladding	Cm
r_{cool}	Effective radius of coolant around fuel pin	Cm

Symbol	Definition	Units
Δr	Radial width of node within fuel	Cm
Δr_c	Radial width of cladding	Cm
Δr_{cool}	Radial width of coolant around fuel pin	Cm
$\vec{R}$	The three spacial variables of core	Cm
$s(z)$	Axial power distribution within fuel pin	Watts/cm^3
$S(\vec{R})$	Spacial power distribution within core	Watts/cm^3
t	Time	Seconds
T_i^j	Temperature (subscript i refers to radial node and superscript j refers to axial node)	^oK
$T_{i_o}^j$	Temperature of radial node i and axial node j at operating level	^oK
$\bar{T}_o^j$	Average fuel temperature of j^{th} segment at operating level	^oK
$\bar{T}_o$	Average fuel temperature of fuel pin at operating level	^oK
$\bar{T}_c^j$	Average coolant temperature of the j^{th} axial segment	^oK
T_c^j	Temperature of coolant at outlet of j^{th} axial segment	^oK
T_c^{j-1}	Temperature of coolant at inlet of j^{th} axial segment	^oK
$\Delta\bar{T}_f$	Change in average fuel temperature of fuel pin	^oK
$\Delta\bar{T}_c^j$	Change in average coolant temperature of j^{th} axial segment	^oK

Symbol	Definition	Units
$\Delta\bar{T}_f^j$	Change in average fuel temperature of j^{th} axial segment	^oK
$\Delta\bar{T}_c$	Change in coolant temperature of fuel pin	^oK
W_1^j	Fuel weighting factor of j^{th} axial segment	Pure number
W_2^j	Coolant weighting factor of j^{th} axial segment	Pure number
z	Axial variable of fuel pin	Cm
Δz	Height of axial node	Cm
β_i	Delayed neutron fraction from i^{th} precursor	Pure number
β	Delayed neutron fraction	Pure number
λ_i	Decay constant for i^{th} precursor	Sec^{-1}
λ	Decay constant for the assumed one precursor	Sec^{-1}
ρ_e	Reactivity due to controlled disturbance	Reactivity units
ρ_f	Reactivity due to feedback	Reactivity units
ρ	Reactivity (subscript Dopp refers to Doppler effect, exp to fuel expansion, and cool refers to coolant expansion)	Reactivity units
$\psi(R)$	Space dependent part of neutron density	Pure number

ACKNOWLEDGEMENT

The author wishes to thank Mr. R. L. Limes, supervisor, computer laboratory, Department of Electrical Engineering, Naval Postgraduate School for his patient help throughout this project, and to Professor C. K. Sanathanan of the University of Illinois, Chicago, for the information supplied through correspondence. Also to Professor A. Gerba for his invaluable assistance and direction.

I. INTRODUCTION

For over twenty years the nuclear community in the U. S. has been working to meet the recognized important objectives of economic nuclear power and improved fuel utilization through the development of the Liquid Metal Fast Breeder Reactor [Ref. 1]. This effort, however, has been largely dispersed with no real organized effort. Starting in 1965 an unprecedented demand for light water reactor power plants occurred paralleled with increased uranium needs. This increased fuel requirement emphasized the need to develop a Liquid Metal Fast Breeder Reactor and has caused the U. S. as well as other countries to establish Liquid Metal Fast Breeder Reactor (LMFBR) programs.

The light water reactors are very successful today with favorable prediction of continued improvements in fuel performance and reduced operating cost [Ref. 2]. However, the LMFBR can provide the most efficient means of exploiting the energy available in uranium because of a high thermodynamic efficiency, an efficient fuel conversion cycle, reasonable capital and operating costs, and safety in operation.

The present U. S. effort in Fast Reactors is summed up in the nuclear reactors Clementine (0.025 Megawatts), LAMPRE I (1 Megawatt), EBR-I (1.4 Megawatts), EBR-II (62.5 Megawatts) and Enrico Fermi (200 Megawatts) of which only the latter two remain in commission. The current LMFBR program envisions a 1,000 Megawatt electric reactor, which is a substantial increase over the largest system constructed to date. It is generally accepted [Ref. 3 and 4] that the operating condition of the proposed LMFBR is beyond the range which permit prudent extrapolation from existing experiences. Simulation studies can greatly

assist in design evaluation by predicting the behavior of the composite model based on experimental information obtained from the component parts.

The use of hybrid simulation is a very effective method to carry out design evaluation based upon the transient response to predictable accidental disturbances. The pure analog approach is not practical due to the prohibited amount of hardware required to simulate the coupled nonlinear differential equations of heat flow. The pure digital approach, which is feasible, does not readily lend itself to multiple parameter studies for design optimization; the computer time required would be economically unfeasible. The hybrid computer combines some of the best characteristics of the analog and digital machines resulting in a more economical computer. Recently, large-scale simulations [Ref. 5 and 6] were performed with the object of comparing the economics of hybrid versus digital for large plant simulation. These simulations indicate that this advantage is not about to disappear.

Previous efforts have been made to demonstrate the feasibility of employing a hybrid computer for the analysis of the transient behavior of a LMFBR core [Ref. 7]. The development of new techniques to enhance the effectiveness of the hybrid computer are currently in progress [Ref. 8]. The method developed in this report is a contribution in this effort with regards to software design related to reducing the number of iterations for convergence. The number of iterations is critical in a hybrid simulation since a large number of iterations would defeat the purpose of using the hybrid computer. A pure digital approach would then become more practical where both discrete time and discrete space could be employed.

Additional contributions were realized by simulating the nonlinear thermal conductivity of UO_2 on a Diode Function Generator resulting in a reduction of analog hardware, and simplification of the neutron kinetics equations for use on the analog computer.

The parameters for the model used are primarily from a recently proposed 1000 MWe LMFBR design [Ref. 9]. However the model developed is quite general and can be employed in the analysis and design studies of fast, intermediate or thermal reactors.

II. DESCRIPTION OF MODEL

A. REACTOR KINETICS

The point reactor kinetics equations are used to describe the neutron density behavior. The assumption is made that the density (F) can be separated into a time dependent and a space dependent term, and can be expressed as[1]

$$F = \psi(\vec{R})\, n(t) \tag{1}$$

Reference 10 and 11 present good treatments of the separation of time and space of the neutron density. n(t) is given by the following equations

$$\frac{dn(t)}{dt} = \frac{1}{\ell}\left[\rho(t) - \beta\right] n(t) + \sum_{i=1}^{N} \lambda_i c_i(t) \tag{2a}$$

$$\frac{dc_i(t)}{dt} = \frac{\beta_i}{\ell}\, n(t) - \lambda_i c_i(t) \tag{2b}$$

where $\beta = \sum_{i=1}^{N} \beta_i$ and with initial conditions $n(0) = \frac{\lambda_i \ell}{\beta_i} c_i(0)$. A treatment of the point reactor kinetics can also be found in Ref. 10 and 11.

In most applications of the above equations it is considered appropriate to treat N = 6, that is 6 delayed neutron precursors. However, in this model due to lack of sufficient analog hardware only one delayed precursor will be considered; its parameters will be appropriate averages of those of the six.

---

[1] R refers to the three spacial variables of the core and not to be confused with r, the radial variable of one fuel pin.

Equation (2) is recast into a more convenient form by defining two dimensionless quantities (see Appendix A for details)

$$N(t) \equiv \frac{n(t)}{n(0)} \quad \text{and} \quad D(t) \equiv \frac{c(t)}{c(0)} .$$

With these definitions and the one precursor assumption equation (2) becomes

$$\frac{d N(t)}{dt} = \frac{\beta}{\ell} \left[K(t) N(t) - N(t) + D(t) \right] \tag{3a}$$

$$\frac{d D(t)}{dt} = \lambda \left[N(t) - D(t) \right] \tag{3b}$$

with initial conditions $N(0) = D(0) = 1$, and where the term $K(t)$ equals $\rho(t)/\beta$ and is defined in dollar units. $\rho(t)$ is the sum of the forcing function $\rho_e(t)$, plus the feedback reactivity $\rho_t(t)$, or simply

$$\rho(t) = \rho_e(t) + \rho_t(t) \tag{4}$$

The quantity β/ℓ for a fast reactor is of the order 10^4, thus equation (3a) requires a high gain integrator for similation on the analog computer. This introduces some problems in the simulation which will be discussed in Section V. If equation (3a) is rearranged as follows,

$$0 = K(t) N(t) - N(t) + D(t) - \left(\ell/\beta\right) \dot{N}(t)$$

the term $\left(\ell/\beta\right) \dot{N}(t)$ represents a small quantity compared to the other three terms of the equation. Neglecting this term is a reasonable approximation and equations (3a) and (3b) become

$$N(t) = K(t) N(t) + D(t) \tag{5a}$$

$$\frac{d D(t)}{d t} = \lambda \left[N(t) - D(t) \right] \tag{5b}$$

Equation (5b) is an initial value ordinary differential equation and its solution is easily handled by the analog computer.

The forcing function is an arbitrary selected but known function of time. In this report a terminated ramp is used to model the withdrawal of a control rod. The feedback reactivity is not a known function of time but depends on the average temperature of the reactor. In a fast reactor there are three main contributions to the feedback [Ref. 12], the Doppler effect, fuel expansion and coolant expansion. The expression for feedback due to these three effects can be represented as[2],

$$\rho_f(t) = -A_{Dopp} \ln\left(1 + \frac{\Delta\bar{T}_f}{\bar{T}_o}\right) - B_{exp}\,\Delta\bar{T}_f + C_{cool}\,\Delta\bar{T}_c$$

or, in terms of dollar units

$$K_f(t) = -\frac{A_{Dopp}}{\beta} \ln\left(1 + \frac{\Delta\bar{T}_f}{\bar{T}_o}\right) - \frac{B_{exp}}{\beta}\,\Delta\bar{T}_f + \frac{C_{cool}}{\beta}\,\Delta\bar{T}_c \qquad (6)$$

A_{Dopp}, B_{exp} and C_{cool} are positive constants. The temperatures indicated in equation (6) represent average core temperatures.

In this model a single average fuel cell is assumed to give all the temperature information necessary to construct the average core temperature.[3]

The power per unit volume supplied by the fission process can be expressed as

$$Q = N(t)\, S(\vec{R})$$

where $S(\vec{R})$ is proportional to $\psi(\vec{R})$. The proportionality factors include

---

[2] See Appendix A for more details.

[3] References 8, 13 and 14 all employ a single "average" fuel cell to compute the reactivity feedback. Reference 7 uses five fuel cells properly weighted to compute the reactivity feedback.

$\nu(0)$, Σ_f (average fission cross section), E (energy released per fission), and V (the average velocity of the neutrons). In this model E, Σ_f and V are treated as constants.

B. HEAT FLOW

Large power densities exist within the core of a 1000 MWe LMFBR giving rise to steep temperature gradients and extreme heat flow. Furthermore the thermal conductivity of the ceramic fuels being considered for the 1000 MWe LMFBR (namely, oxides, nitrites and carbides) vary nonlinearly at the proposed high operating temperatures. These factors dictate that the problem of heat flow be approached on a microscopic basis.

A LMFBR is composed of thousands of pencil size fuel pins approximately three feet long in the shape of right cylinders; the coolant flows coaxially. A sample fuel pin illustrated in Fig. 1 is composed of a cylindrical shaped fuel assembly with a concentric shell called cladding.

The heat flow equation for a cylindrical shaped body with varying thermal properties is:

$$cd\,\frac{\partial T}{\partial t} = \frac{1}{r}\left\{\frac{\partial}{\partial r}\left[K(T)\,r\,\frac{\partial T}{\partial r}\right] + \frac{\partial}{\partial \theta}\left[K(T)\,\frac{1}{r}\,\frac{\partial T}{\partial \theta}\right] + \frac{\partial}{\partial z}\left[r\,K(T)\,\frac{\partial T}{\partial z}\right]\right\} + Q(r,\theta,z,t) \tag{8}$$

In a fast reactor the neutron flux is nearly constant within the fuel pin in the radial direction (in contrast to a thermal reactor where flux depression occurs within the fuel). This fact gives rise to cylindrical symmetry and if axial flow of heat is neglected, which is consistant with other models proposed [Ref. 5, 13 and 14], equation (8) for any fuel pin reduces to:

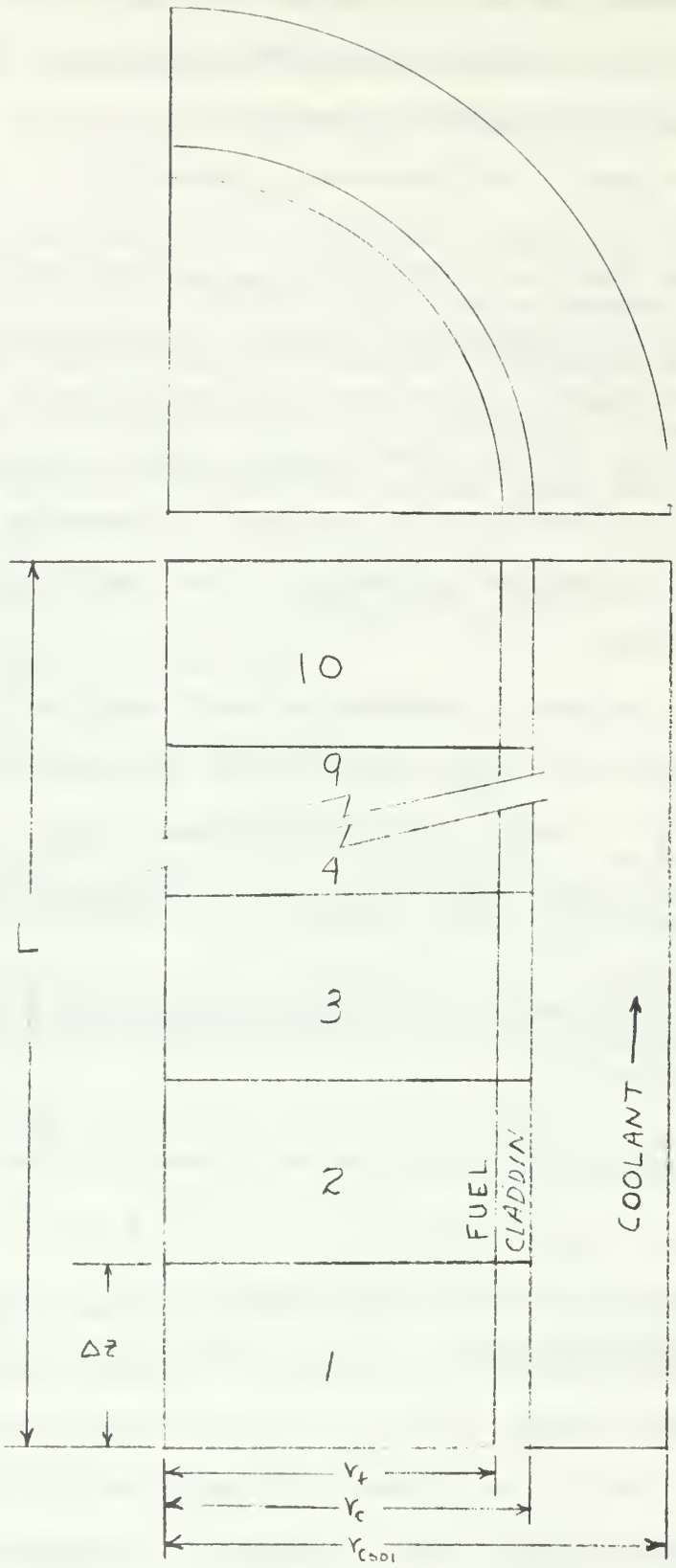

Figure 1. Diagram of Fuel Pin

Fuel: $$c_f d_f \frac{\partial T}{\partial t} = \frac{1}{r} \frac{\partial}{\partial r} \left[r K_f(T) \frac{\partial T}{\partial r} \right] + s(z) N(t) \qquad (9)$$

Cladding: $$c_c d_c \frac{\partial T}{\partial t} = \frac{1}{r} \frac{\partial}{\partial r} \left[r K_c(T) \frac{\partial T}{\partial r} \right] \qquad (10)$$

where the assumptions outlined in Section IIA for the power generation Q, have been introduced (i.e, the space and time separation of neutron density). The term $S(\vec{R})$ has been replaced by $s(z)$ to indicate the heat generation rate in a single fuel pin is a function of the axial direction only.

Since the analog computer can handle only ordinary differential equations, equations (9) and (10) are reduced to initial value ordinary differential equations by employing a method of integrating over the spacial variable [Ref. 15]. The technique involves discretizing the space variable in the radial direction, r, into five nodes within the fuel and one within the cladding (see Fig. 2). In carrying out the integration the temperature is assumed to vary linearly between nodes. For more details of the derivations refer to Appendix A.

As a result of employing this technique equations (9) and (10) become:

$$\text{Fuel:} \quad c_f d_f \frac{d}{dt} \left[\left(\frac{1}{8} - \frac{\Delta r}{24 r_i} \right) T_{i-1}^j + \frac{3}{4} T_i^j + \left(\frac{1}{8} + \frac{\Delta r}{24 r_i} \right) T_{i+1}^j \right]$$

$$= K_{f,i+1,i} \left(1 + \frac{\Delta r}{2 r_i} \right) \left(\frac{T_{i+1}^j - T_i^j}{\Delta r^2} \right) \qquad (11)$$

$$- K_{f,i,i-1} \left(1 - \frac{\Delta r}{2 r_i} \right) \left(\frac{T_i^j - T_{i-1}^j}{\Delta r^2} \right) + s(z) N(t)$$

(i indicates the node which varies in number from 1-5 within the fuel)

$K_{f,i,i+1}$ = thermal conductivity at boundary between node i and i + 1

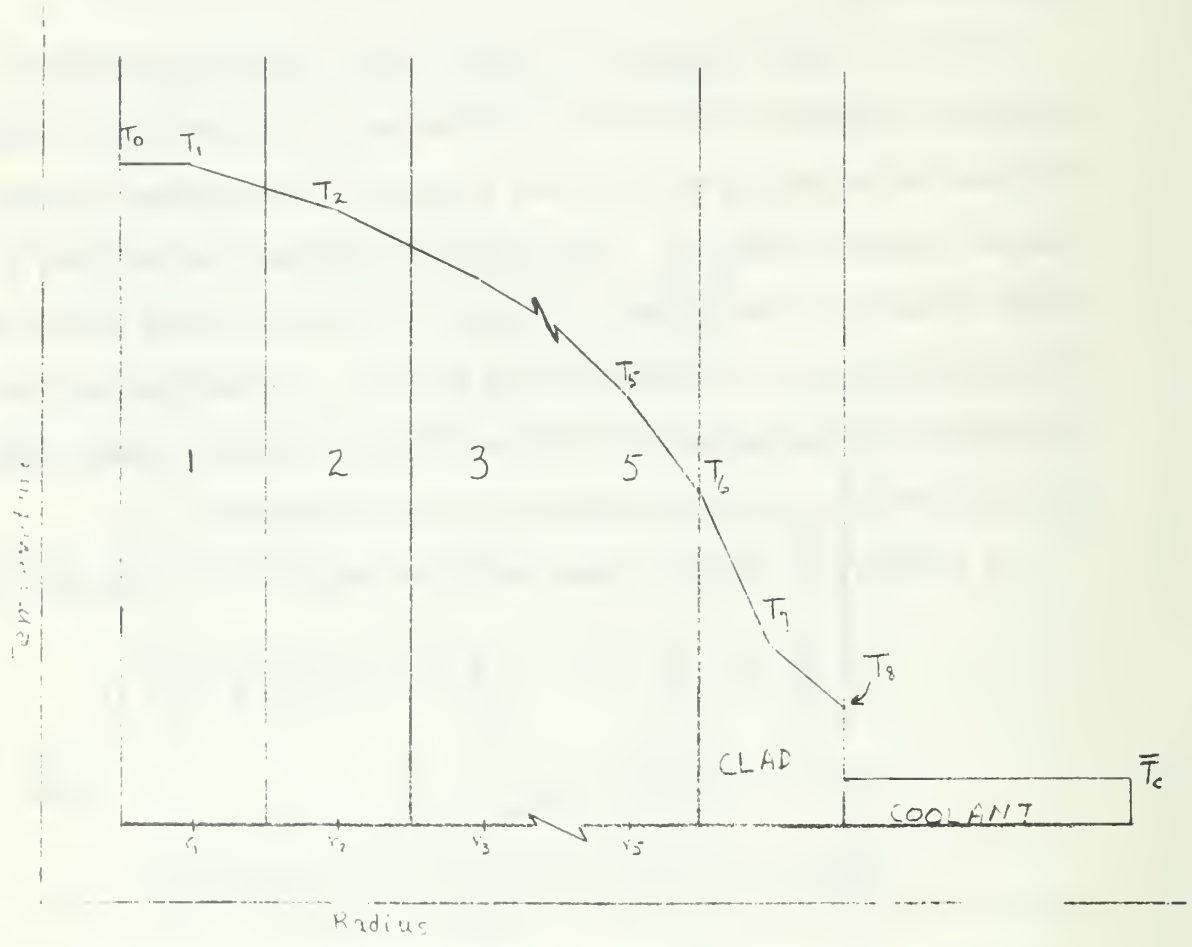

Figure 2. Temperature Profile Assumed Within Fuel Pin.

Cladding: $$C_c d_c \frac{d}{dt}\left[T_6^j\left(\frac{1}{4}-\frac{\Delta r_c}{12 r_6}\right)+\frac{1}{2}T_7^j+T_8^j\left(\frac{1}{4}+\frac{\Delta r_c}{12 r_6}\right)\right]$$

$$= K_c\left(1+\frac{1}{2r_6}\right)\left(\frac{T_6-T_7}{\Delta r_c^2/2}\right) \qquad (12)$$

$$- K_c\left(1-\frac{1}{2r_6}\right)\left(\frac{T_7-T_8}{\Delta r_c/2}\right)$$

(Superscript j refers to the axial node)

Due to symmetry about r = 0, the condition that $T_0^j = T_1^j$ is applied as a boundary condition. Also at the clad-fuel interface the continuity of heat flow requires that

$$K_{f,6}\left(\frac{T_6^j - T_8^j}{\Delta r/2}\right) = K_c\left(\frac{T_7^j - T_8^j}{\Delta r_c/2}\right)$$

At the boundary between cladding and coolant the conservation of energy is applied to arrive at the following equation (see Appendix A for derivation).

$$\frac{\partial T_c}{\partial t} + \frac{G(t)}{d_{cool}}\frac{\partial T_c}{\partial z} = \frac{2H}{r_c C_{cool} d_{cool}} \qquad (13)$$

$G(t) \equiv$ mass flow rate of coolant

$H \equiv$ heat flux across the clad-coolant interface

$r_c \equiv$ radius of fuel pin (fuel + cladding)

Again an ordinary differential equation is needed. Here, however, the use of finite differencing of the space variable is more practical. This simply requires replacing $\partial T_c/\partial z$ by $(T_c^j - T_c^{j-1})/\Delta z$ and assuming the coolant temperature varies linearly over length Δz. Thus equation (13) can be expressed as:

$$\frac{d\bar{T}_c^j}{dt} + \frac{G(t)}{d_{cool}\Delta z}\left(T_c^j - T_c^{j-1}\right) = \frac{2H}{r_c C_{cool} d_{cool}}$$

$\bar{T}_c^j \equiv$ average coolant temperature of j^{th} axial segment $= \frac{T_c^j + T_c^{j-1}}{2}$

At the clad-coolant boundary the heat flow per unit time (H) is represented by $h(T_s - \bar{T}_c)$ which also equals $K_c \left(\frac{T_7 - T_8}{\Delta r_c/2}\right)$. h is the heat transfer coefficient between clad and coolant.

After incorporating the boundary conditions and the physical constants listed in Appendix C the following coupled ordinary differential equations are obtained.

$$\frac{d}{dt}\left[T_1^j + .2633 T_2^j\right] = 328.2\left[K_{f,1,2}(T_2^j - T_1^j)\right] + .41\, s(z)\, N(t) \tag{15}$$

$$\frac{d}{dt}\left[T_2^j + .2032 T_3^j + .1295 T_1^j\right] = 231.0\left[K_{f,2,3}(T_3^j - T_2^j)\right] - 115.5\left[K_{f,1,2}(T_2^j - T_1^j)\right] + .433\, s(z)\, N(t) \tag{16}$$

$$\frac{d}{dt}\left[T_3^j + .1889 T_4^j + .1494 T_2^j\right] = 208.0\left[K_{f,4,3}(T_4^j - T_3^j)\right] - 138.8\left[K_{f,3,2}(T_3^j - T_2^j)\right] + .433\, s(z)\, N(t) \tag{17}$$

$$\frac{d}{dt}\left[T_4^j + .1826 T_5^j + .1507 T_3^j\right] = 198.1\left[K_{f,5,4}(T_5^j - T_4^j)\right] - 148.5\left[K_{f,4,3}(T_4^j - T_3^j)\right] + .433\, s(z)\, N(t) \tag{18}$$

$$\frac{d}{dt}\left[T_5^j + .1880 T_4^j + .4362 T_6^j\right] = 469.0\left[K_{f,6}(T_6^j - T_5^j)\right] - 187.5\left[K_{f,5,4}(T_5^j - T_4^j)\right] + .528\, s(z)\, N(t) \tag{19}$$

$$\frac{d}{dt}\left[T_8^j + 1.385 T_7^j + .885 T_6^j\right] = 174.1\left[T_8^j - T_7^j\right] - 698.0\left[K_{f,6}(T_6^j - T_5^j)\right] \tag{20}$$

$$\frac{d}{dt}\bar{T}_c^j = -186.3\,\bar{T}_c^j + 118.8\, T_8^j + 67.5\, T_c^{j-1} \tag{21}$$

The inlet temperature to the first axial segment is known and treated as a constant during any transient. In nuclear reactors the inlet temperatures are usually kept constant, and any rapid power change will have leveled off before any change occurs in the inlet temperature. For each subsequent segments the inlet temperature is a known function of time obtained from analysis of the previous section (see Digital Software section for details). The steady state spacial power distribution $s(z)$ is known a priori, therefore, equations (15) through (21) can be solved on the analog computer.

The bonding between the fuel and cladding is ignored in this model and the fuel is assumed to be in constant contact with the cladding. In most LMFBR under design the bonding agent is helium. Neglecting this bonding will produce lower than normal temperatures within the fuel.

III. HYBRID COMPUTER TECHNIQUE

A. DESCRIPTION OF ANALOG COMPUTER HARDWARE

From the heat flow equations given in the previous section it can be seen that the model requires the simulation of a large number of ordinary differential equations. However, an important aspect to keep in mind is that the description of each axial segment incorporates the same differential equations, the coolant inlet temperature and the fuel heat generation rate being the only quantities varying from segment to segment. With this in mind a technique of multiplexing that is, time sharing, of the analog circuitry can be employed. The details of the multiplexing used will be explained in Section IIIB. To use the technique, only one set of equations (15) through (21) need be set up on the analog computer. In order to solve equations (15) through (21) on the analog computer they must first be magnitude scaled to insure that the outputs do not exceed the maximum analog computer voltage ($\pm$ 100^{V}). After proper scaling equations (15) through (21) can be expressed as equations (41) through (47) which are shown in Appendix B.

The approach used in setting up the solution to equations (41) through (47) on the analog computer can best be explained by taking one equation,

$$\frac{d}{dt}\left[\bar{T}_2^j + .2038\,\bar{T}_3^j + .1295\,\bar{T}_1^j\right] = 23.1\left[10\,\bar{K}_{f,2,3}\left(\bar{T}_3^j - \bar{T}_2^j\right)\right] - 11.55\left[10\,\bar{K}_{f,1,2}\left(\bar{T}_2^j - \bar{T}_1^j\right)\right] + .2165\,\bar{S}(z)\,\bar{N}(t) \tag{42}$$

The right side of equations (42) represents inputs to an integrator whose analog symbol is shown by element A in Fig. 3. Element B is a summer amplifier. This process is extended over the remaining heat equations. Figure 4a is a diagram of the analog circuitry.

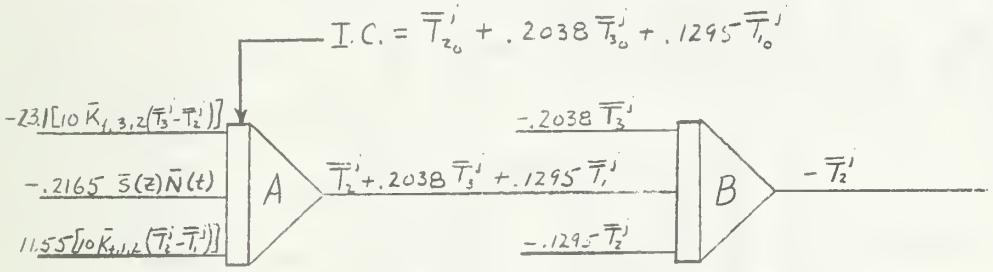

I.C. refers to initial conditions.

Figure 3. Illustration of Technique Used to Construct Analog Circuit.

The nonlinearity of the thermal conductivity, K(T), was readily handled by the analog computer through utilization of a Diode Function Generator (DFG). A DFG can be used to approximate a nonlinear curve by the method of straight line segments. The DFG used with this simulation has ten break points. Thus a maximum of ten straight lines were available to duplicate the curve and this was quite adequate to give a good representation of the nonlinearity. Experimental data for the K(T) curve was obtained from Ref. 16 and 17. Figure 5 shows both curves. The DFG operates simply as shown in Fig. 6. The input is a voltage which represents ^{o}K temperature and the output is a voltage proportional to the thermal conductivity for that temperature

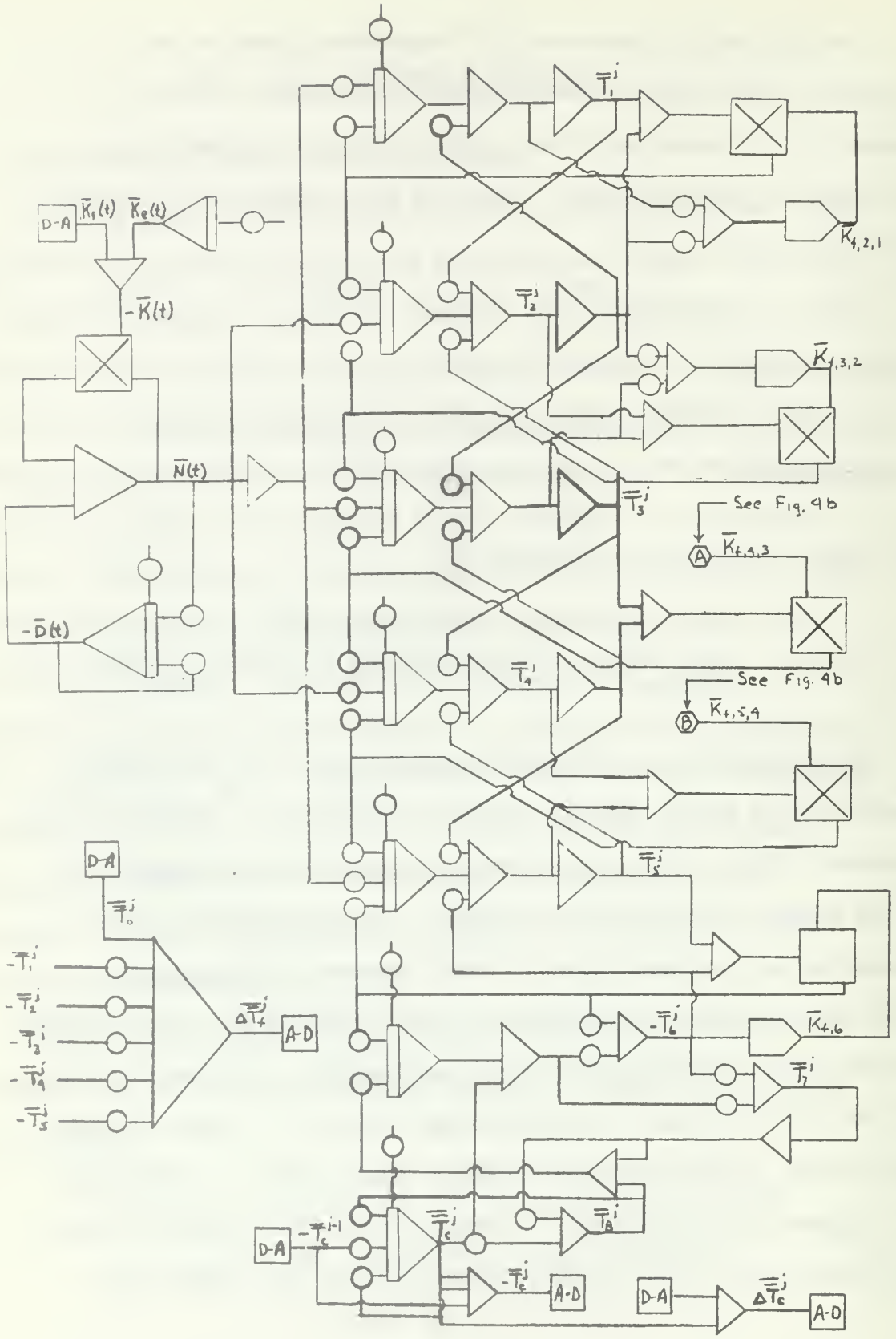

Figure 4a. Diagram of Analog Circuit.

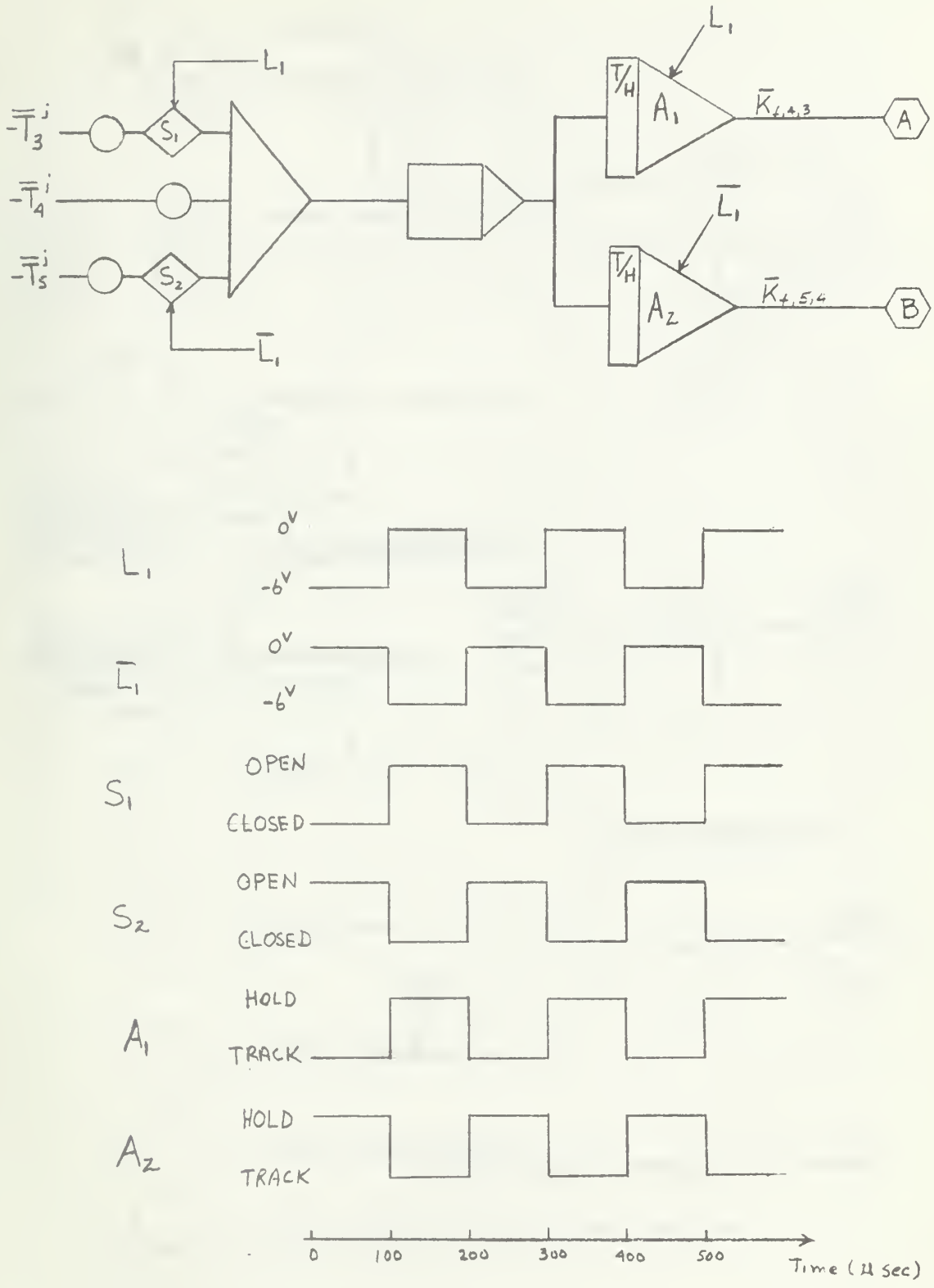

Figure 4b. Diagram of Multiplexed DFG.

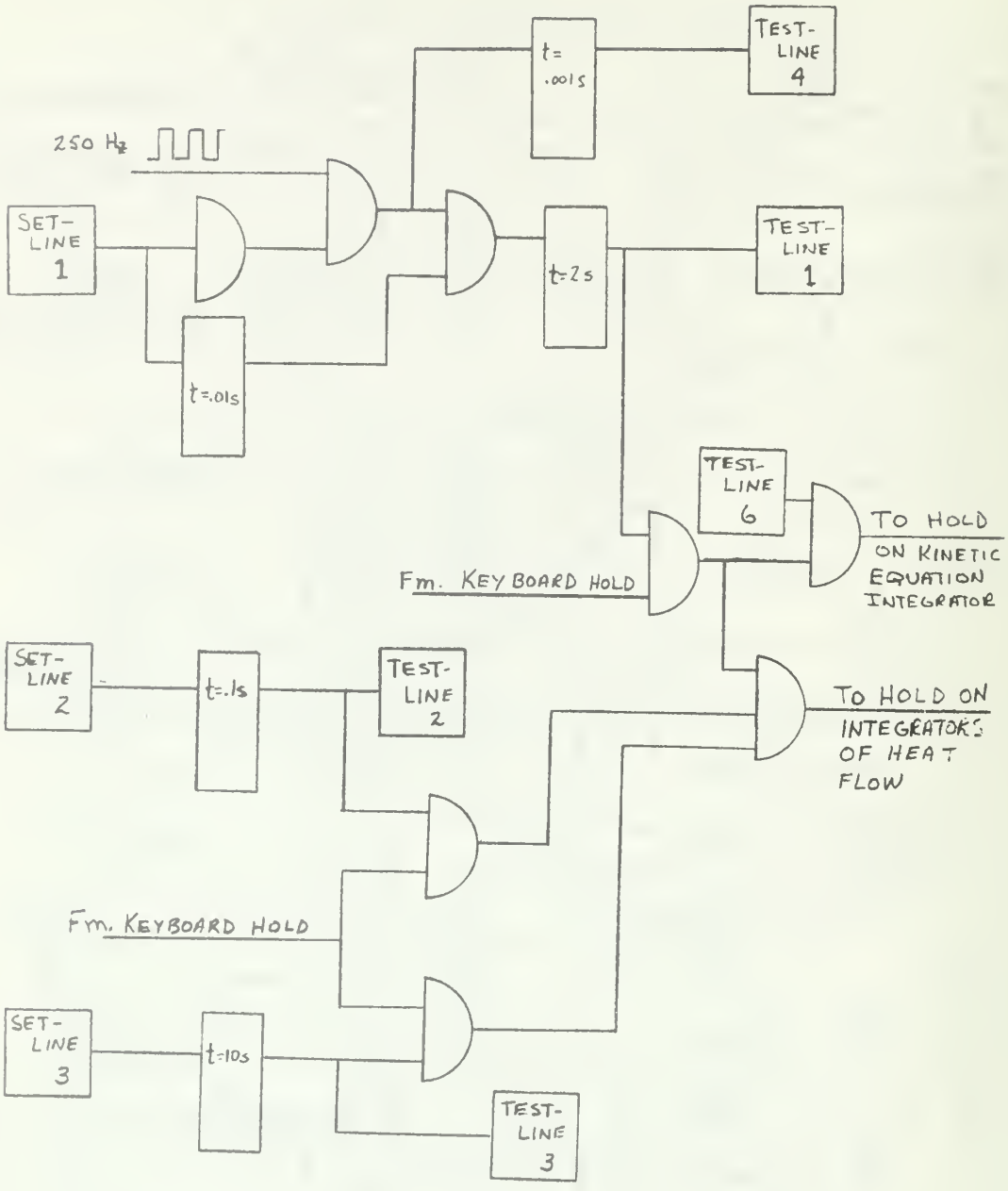

Figure 4c. Diagram of Logic Circuit.

Integrator

Summer amplifier

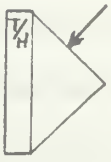

Track-hold amplifier

Analog multiplier

Potentiometer

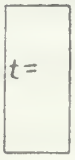

Delay flop

Nand-gate

Diode Function Generator

Analog/digital switch

Input or output from digital computer

Figure 4d. Key For Analog Symbols.

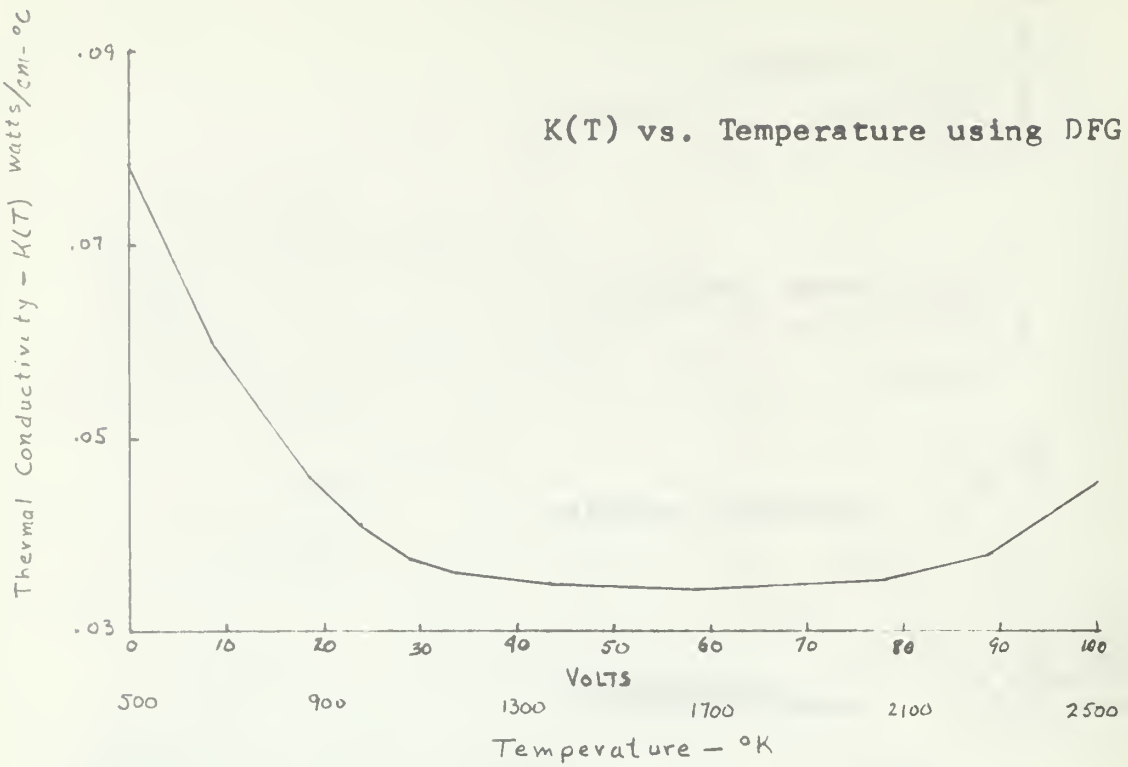

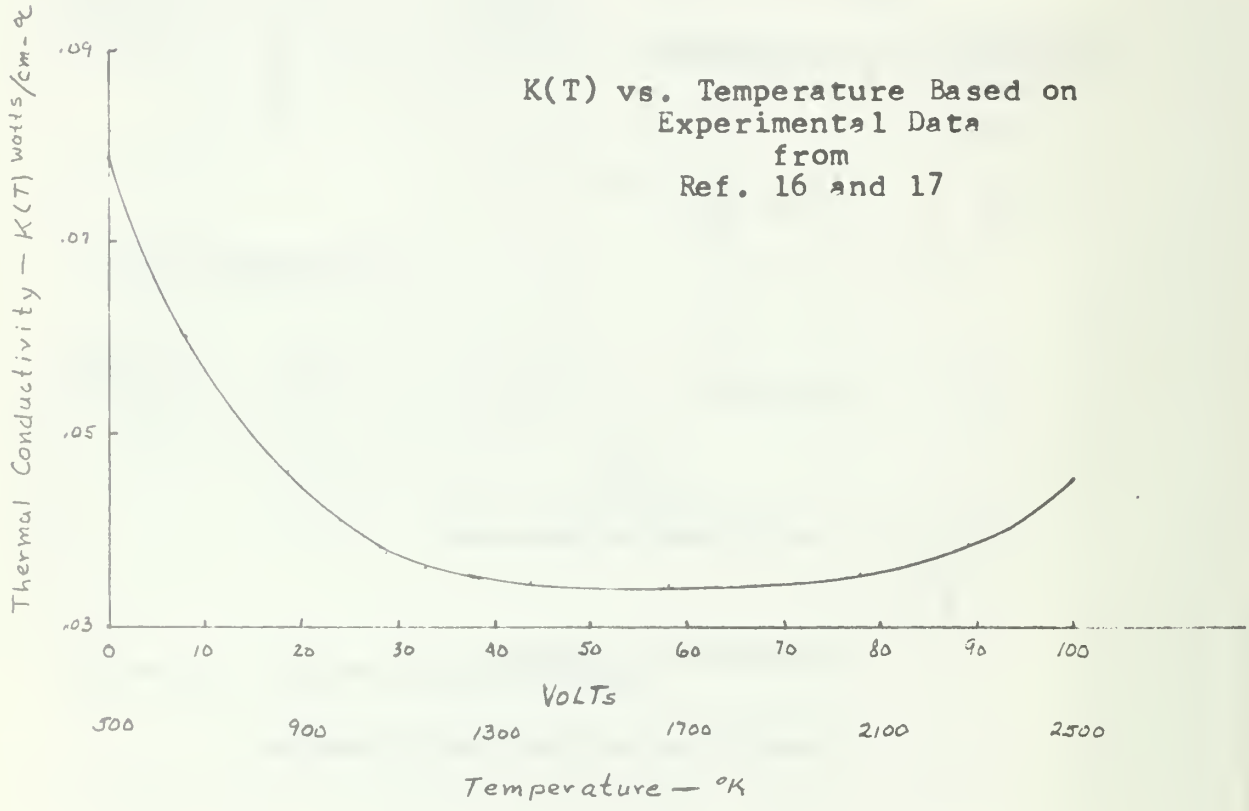

Figure 5. Thermal Conductivity Of UO_2.

Figure 6. Block diagram of DFG.

The boundary conditions of the five fuel nodes required five values of K(T). However only four DFG's were available on the analog computer, consequently, one of the DFG's had to be time shared. The time sharing was accomplished by alternating the information to a DFG from two boundaries. The switching was accomplished by two digital/analog switches. The logic to operate one of the switches was supplied by a 10 kHz square wave which for clarity will be called logic variable L_1; the other switch was operated by $\bar{L}_1$, the inversion of L_1. The output of the DFG was fed to two track-hold amplifiers, one being controlled by logic L_1 and the other by $\bar{L}_1$. With the aid of Fig. 4b it can be seen that while one switch is closed one amplifier will be in the track mode following the output of the DFG while the other is in the hold mode. When the logic signal inverts the switches reverse conditions and the amplifiers reverse modes.

The analog computer used for this model, COMCOR-5000, is equipped with digital logic and in addition completely controllable by the general purpose digital computer, SDS-9300. However it was necessary to develop a logic network which could control the compute mode of the analog computer automatically using the digital computer for varying periods of time. Furthermore at times it was necessary to bring the model up to operating temperature before the external forcing function was applied to the reactor kinetics. To realize this flexibility a complete logic network was developed which is shown in Fig. 4c.

B. DESCRIPTION OF DIGITAL COMPUTER SOFTWARE

In the previous section it was pointed out that the solution to the heat flow for the complete fuel pin involved one set of equations by applying the analog circuitry of Fig. 4a on a time sharing basis. The digital computer with its logic capabilities can control this time sharing very effectively. Essentially what occurs is that the analog computer is used as a large subroutine and when called produces the solution for the axial segment under consideration.

In this simulation the solution to one axial segment is treated on a continuous time basis during any transient condition. In order to treat each segment in this manner the time behavior of the inlet coolant temperature must be incorporated within the solution for that segment. The digital computer with its memory capabilities can accomplish this effectively. The digital computer through an analog-digital converter samples at a fast rate (250 Hz) the outlet temperatures of the segment being considered. This information is stored as an array within the digital computer and used as input data in the form of a analog voltage through a first order digital to analog converter during the solution of the next segment. Thus the solution can continue sequentially from one axial segment to the next.

The feedback shown in equation (6) is an algebraic function and for this reason it is more convenient to have the digital computer handle this aspect of the simulation. However, it is necessary at this point to note that the feedback mechanism is a function of the average temperature. This situation requires that the average temperature be known at a given time in order that the digital computer can evaluate the feedback. However the average temperature of the

core is not known until all the segments have been considered. To obtain the average temperature, the average fuel and coolant temperatures of each segment are weighted to approximate the average temperature. Each segment is then evaluated on a continuous time basis with the digital computer supplying the closed-loop feedback. The operation is illustrated in Fig. 7 where the closed-loop system for each axial segment is shown. During the analysis of each segment the digital computer rapidly samples the logic condition, defined L3, on a 250 Hz signal which commences simultaneously with the signal which places the integrators in the compute mode (Fig. 8). When L3 is -6 volts the digital computer samples the change in ambient temperature for the fuel ($\Delta\bar{T}_f^j$) and coolant ($\Delta\bar{T}_c^j$) for the axial segment j being considered, stores the information, computes a feedback after weighting the temperatures, and outputs the feedback just computed as a voltage to the analog computer (Fig. 8c). L3 during the above operation has returned to 0 volts. The digital computer remains in a loop until L3 again has the value -6 volts whereupon the process in Fig. 8c is repeated. The condition of 0 volts on logic signal L2 occurring at time t ends the computation for that segment. For clarity the analysis of all ten segments in this manner will be referred to as iteration 1.

After each segment is analyzed the fuel and coolant temperatures, each represented by a 250 x t matrix, are stored on a disc due to storage limitations within the digital computer. After all ten segments have been analyzed the 10 x 250 x t array for each temperature is processed to obtain a 250 x t array representing the average temperature as a function of time. A $K_f(t)$ is then computed based on

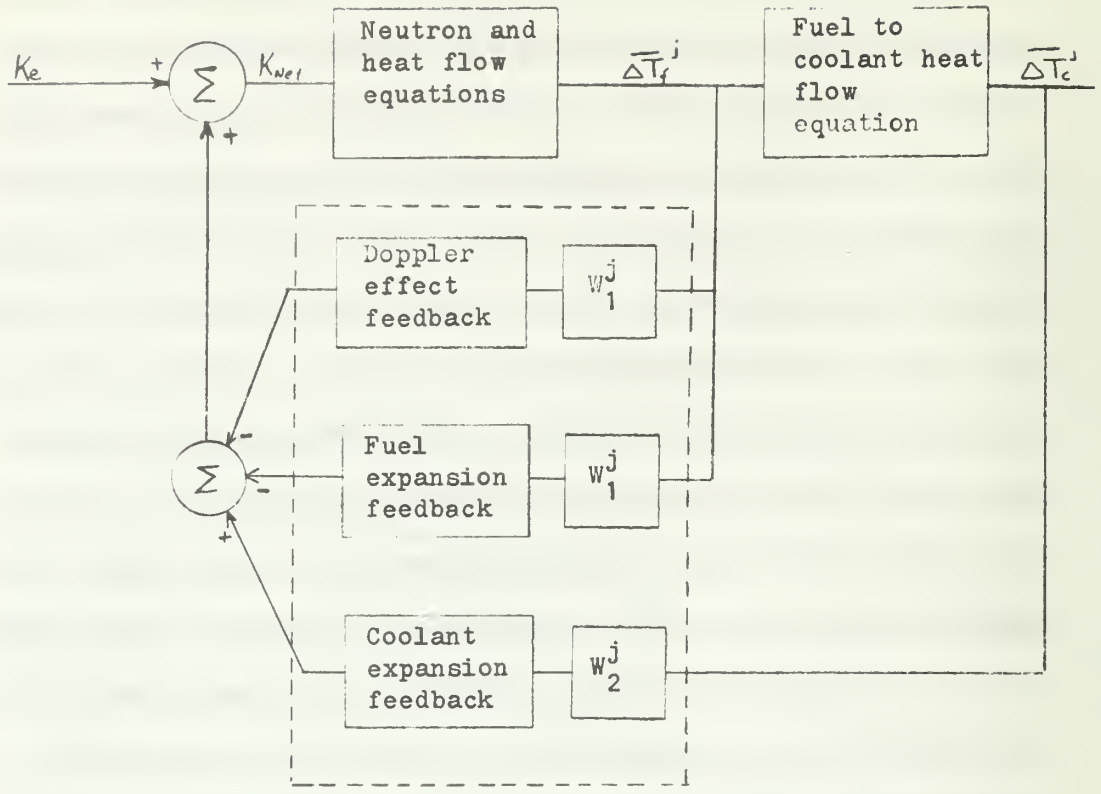

That portion enclosed by dashed lines indicates the part being handled by the digital computer.

Figure 7. Closed-Loop Feedback Schematic for Each Axial Segment.

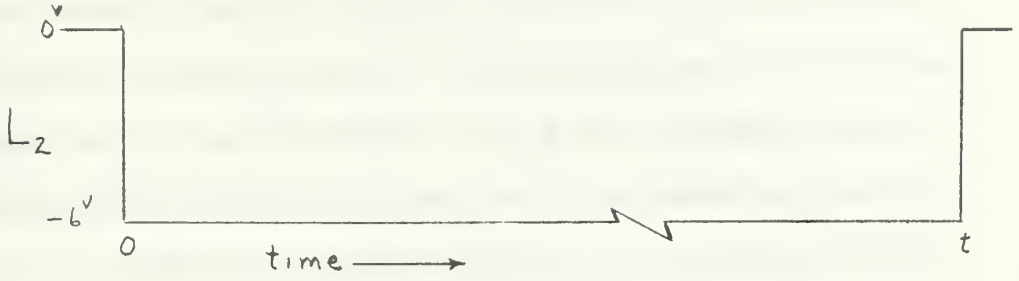

(a)

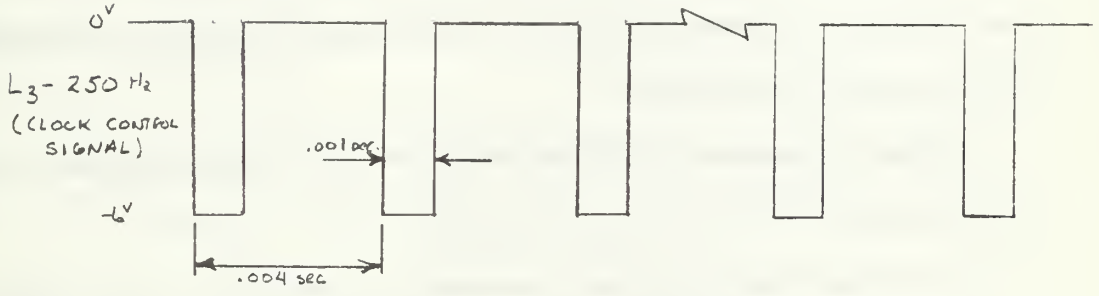

(b)

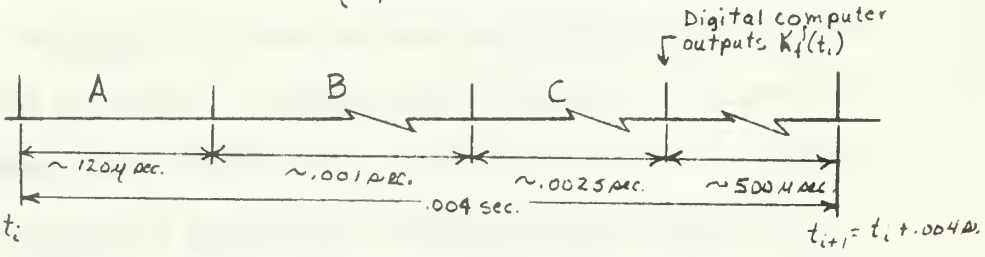

A — duration of test by digital computer on L_3

B — digital computer outputs $T_c^{j-1}(t_i)$ and samples $\Delta\bar{T}_f^j(t_i)$, $\Delta\bar{T}_c^j(t_i)$, and $\bar{T}_c^j(t_i)$, and stores information.

C — digital computer evaluates $K_f(t_i)$ and outputs at conclusion of computation.

(c)

Figure 8. Timing Diagram.

this average temperature. A new iteration is made using the $K_f(t)$ just computed. The changes in fuel and coolant temperatures are sampled as before. However this iteration differs from iteration 1 in that the loop is not closed but open. Figure 9 shows the schematic for the open-loop process. At the conclusion of analyzing the ten axial segments a new $K_f(t)$ is computed based on the temperature profiles just developed. The open loop process is then repeated until convergence of the neutron density N(t) occurs.

When applying the open-loop iterative method, a study should be conducted to insure that convergence will occur before attempting this procedure. Proof that this system will converge is given in Ref. 5 and 18, however Section V of this report covers a discussion on the rate of convergence.

Figure 10 represents a flow chart for the digital software program just outlined.

The method for obtaining the weighting factors for the coolant and fuel temperatures is now described. Normally to start the problem from a known steady-state spacial power distribution, the initial conditions on the itegrators were needed. These were easily obtained by putting in a step input of heat and allowing each segment to come to steady state (operating level). The final voltages on all integrators were sampled and the information put on paper tape for future use as initial conditions. After each segment had reached operating level, it was disturbed with $K_e(t)$ as a ramp input for a short period of time .1 sec) without feedback. The changes in average fuel and coolant temperatures for this time interval were sampled for each j^{th} axial segment and from these temperatures the changes in average coolant

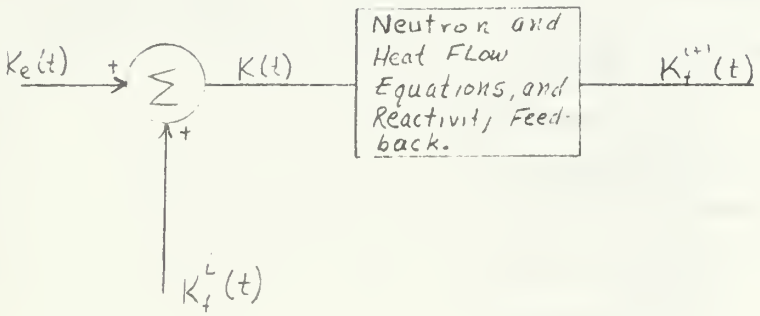

Figure 9. Block Diagram of Open-Loop Process.

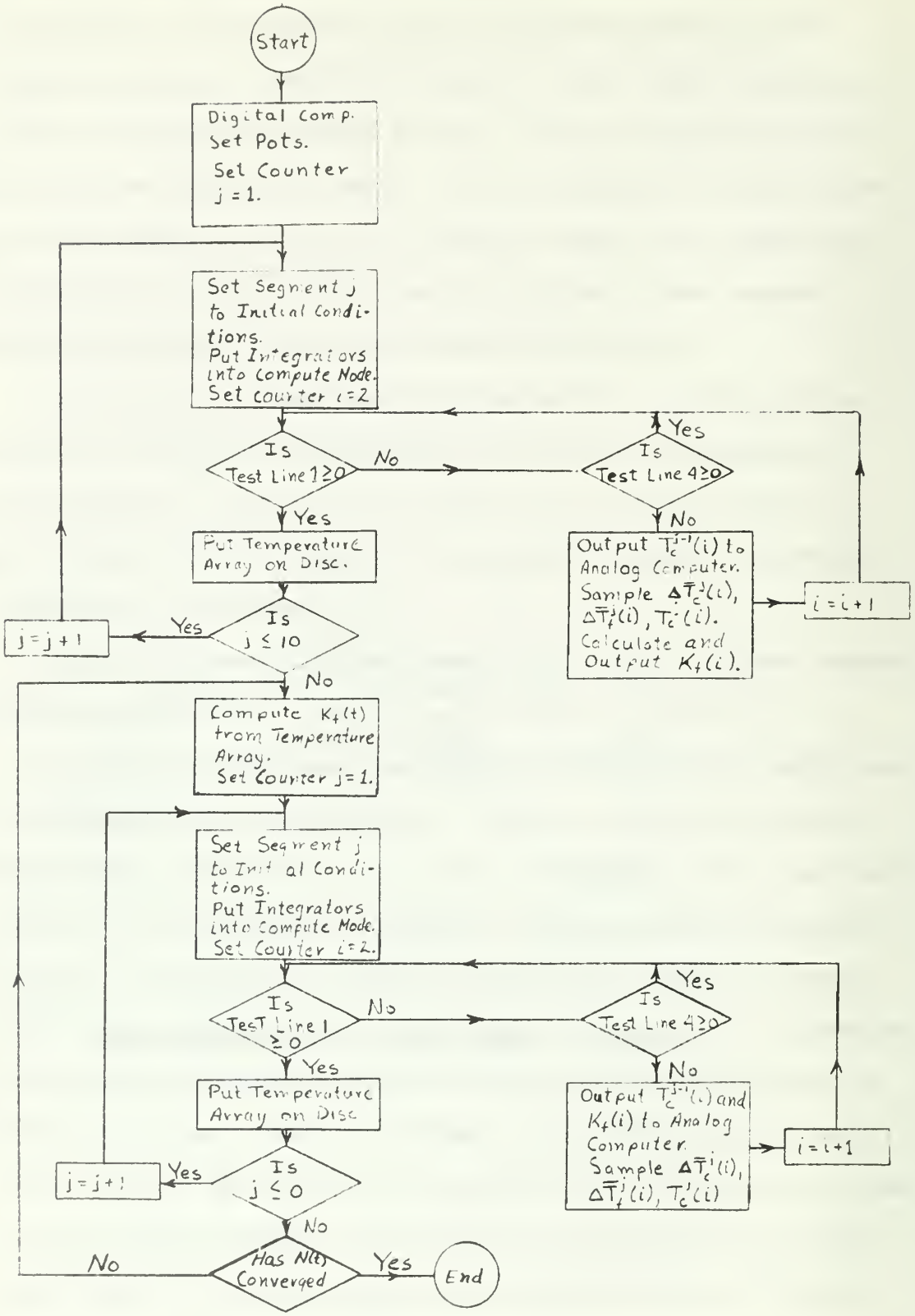

Figure 10. Digital Computer Program Flow Chart.

($\Delta\bar{T}_c$) and fuel ($\Delta\bar{T}_f$) temperatures for the fuel pin were calculated. The weighting factors, W_1^j and W_2^j, were calculated using the following relationships,

$$W_1^j = \frac{\Delta\bar{T}_f}{\Delta\bar{T}_f^j}$$

$$W_2^j = \frac{\Delta\bar{T}_c}{\Delta\bar{T}_c^j}$$

These weighting factors were then treated as constants for the duration of the transient condition.

IV. DYNAMIC CHECK OF MODEL

When a physical system is described by a model it is important to know whether this model is adequately describing the system. To ascertain this, parts of the mathematical model were compared with known mathematical solutions or with digital computer solutions.

The approximated neutron kinetics equations (5) were compared with the exact solution for the case of the one delayed emitter model using a step input of reactivity of magnitude 50 cents. Representing this step input by K_1 the solution of the reactor kinetics can readily be obtained for this input condition [Ref. 19] and is given in equation (22) for the one delayed emitter model.

$$N(t) = \left(\frac{b-c}{b-a}\right) e^{at} + \left(\frac{c-a}{b-a}\right) e^{bt} \tag{22}$$

where,

$$a = \frac{K_1 \lambda}{\frac{\lambda \ell}{\beta} + 1 - K_1}$$

$$b = \frac{K_1 - 1}{\ell/\beta}$$

$$c = \frac{K_1}{\ell/\beta}$$

When practical numbers are used in equation (22) product terms containing λ can be neglected and the solution can be expressed as

$$N(t) = \frac{1}{1-K_1} e^{\left[\frac{\lambda K_1}{1-K_1}\right]t} - \frac{K_1}{1-K_1} e^{\left[\frac{K_1 - 1}{\ell/\beta}\right]t} \tag{22a}$$

Since $\ell/\beta \approx 10^{-4}$ the second exponent has a time constant 2×10^{-4} sec., therefore it is unnoticable on any time scale of interest and to

a good approximation it can be neglected. What occurs with this assumption is that N(t) is a step jump to $\frac{1}{1-K_1}$ instead of delaying $\sim$ .001 sec. Figure 11 shows both the analog solution of equation (5) and the exact solution given in equation (22a). From the results it can be seen that the approximation used to develop equation (5) appears valid.

Equation (5) was also solved on the analog computer using a triangular pulse input for K(t) as follows:

$$K(t) = \begin{cases} .5t \text{ dollars}, & 0 \le t \le 1 \text{ sec.} \\ (1-.5t) \text{ dollars}, & 1 \text{ sec.} < t \le 2 \text{ sec.} \\ 0, & t > 2 \text{ sec.} \end{cases} \qquad (22b)$$

A digital computer integration solution utilizing the Runga-Kutta method with a Adams-Moulton predictor corrector with error check (absolute error $\le 10^{-4}$ per integration step) [Ref. 20 and 21] was also used to solve the reactor kinetics without the approximation, equation (3). The results of both solutions are shown in Fig. 12. Table I shows a comparison between the values for the two solutions for every tenth of a second. The agreement is quite good.

The heat flow equations were solved on the analog computer for a homogeneous material with constant thermal properties. The exterior of the material was kept at a constant temperature and a constant heat source was applied within the material. The solution for this situation, recalling that the equations apply for a circular cylinder, is [Ref. 22]

$$T(t) = \frac{q(a^2-r^2)}{4K} - \frac{2q}{aK} \sum_{n=1}^{\infty} e^{-\frac{K}{cd}\alpha_n^2 t} \left[\frac{J_0(\alpha_n r)}{\alpha_n^3 J_1(\alpha_n a)} \right]$$

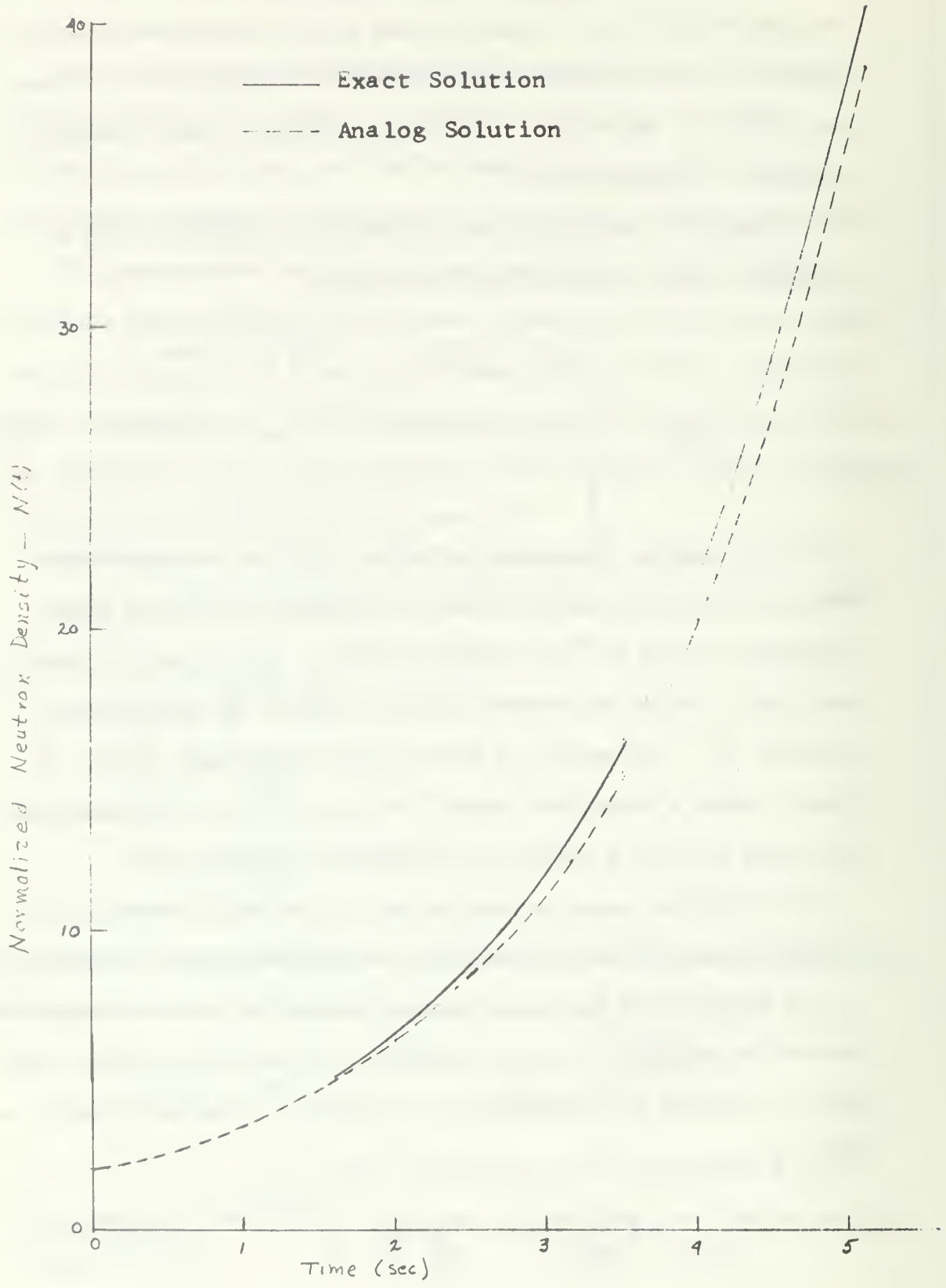

Figure 11. Comparison of Analog And Exact Solution For Neutron Kinetics For a Step Input of 50 Cents.

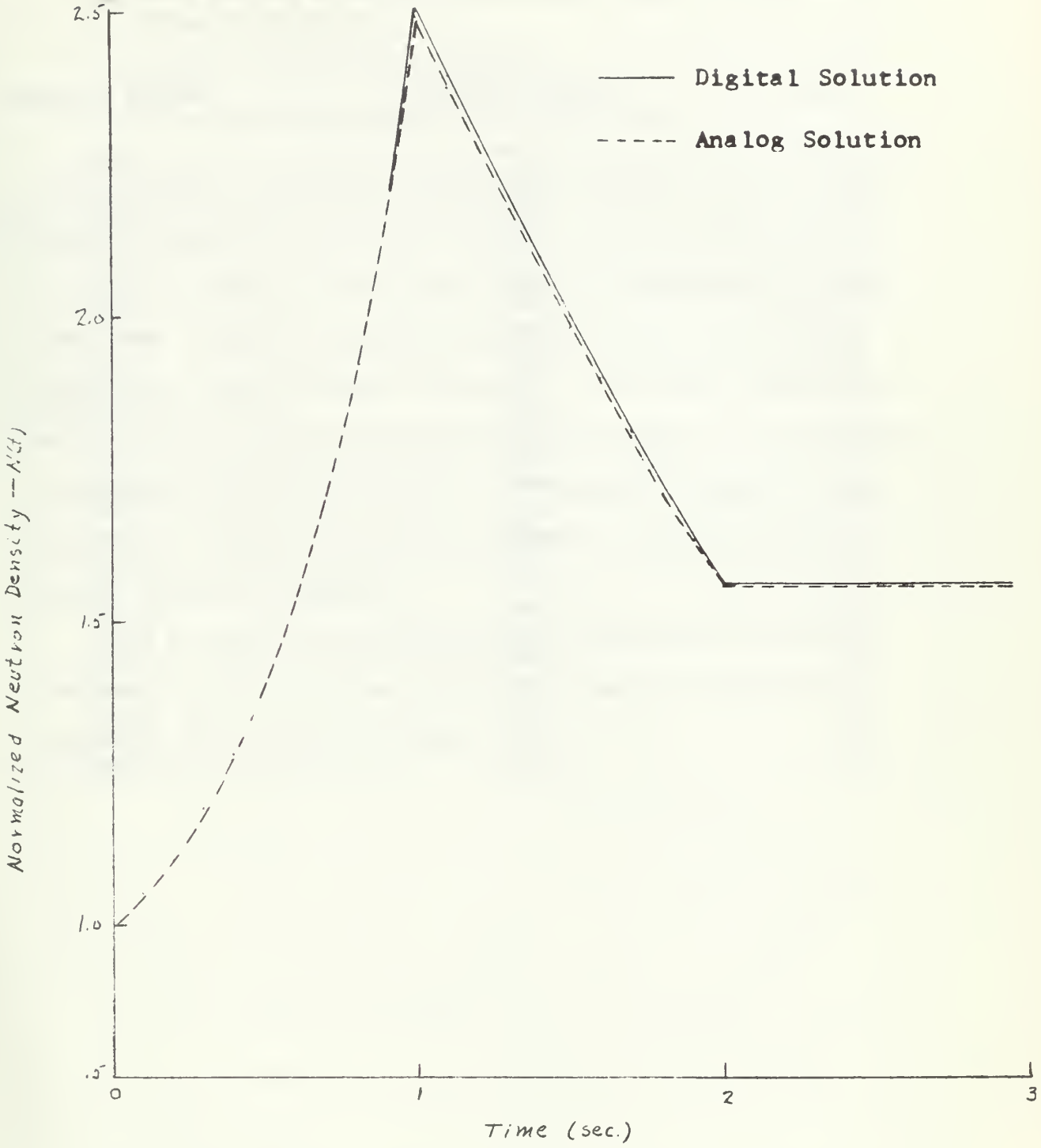

Figure 12. Comparison of Analog and Digital Solution of Neutron Kinetics for a Triangular Pulse Input for K(t).

TABLE I

COMPARISON OF DIGITAL AND ANALOG SOLUTION OF REACTOR KINETICS

Time	Digital solution	Analog solution
0.1	1.054	1.052
0.2	1.118	1.117
0.3	1.194	1.192
0.4	1.284	1.282
0.5	1.393	1.390
0.6	1.525	1.522
0.7	1.689	1.685
0.8	1.895	1.891
0.9	2.157	2.150
1.0	2.501	2.481
1.1	2.398	2.376
1.2	2.295	2.275
1.3	2.194	2.174
1.4	2.095	2.075
1.5	1.999	1.980
1.6	1.906	1.890
1.7	1.816	1.800
1.8	1.730	1.712
1.9	1.646	1.629
2.0	1.566	1.558
2.1	1.566	1.558
2.2	1.566	1.558
2.3	1.566	1.558
2.4	1.566	1.558
2.5	1.566	1.558

where,

q = heat applied in Watts/cm^3

a = radius of cylinder

K = thermal conductivity of material

α_n = n^{th} root of Bessel function of order zero.

Figure 13 shows a comparison between both solutions. It can be seen that the solution is quite good for nodes 1 through 4 but node 5 is in error by as much as 25% in early values of time and 10% in final time. The situation is generally recognized [Ref. 23] as being a problem near abrupt boundary conditions. Since abrupt changes are not envisioned as part of any study with this model it can reasonably be expected this error to be less. Furthermore the average temperature is the important quantity of interest; thus the error will be further reduced in magnitude.

Prior to making any computations with this model it is wise to carry out a static and dynamic check of the model to insure all components are functioning properly.

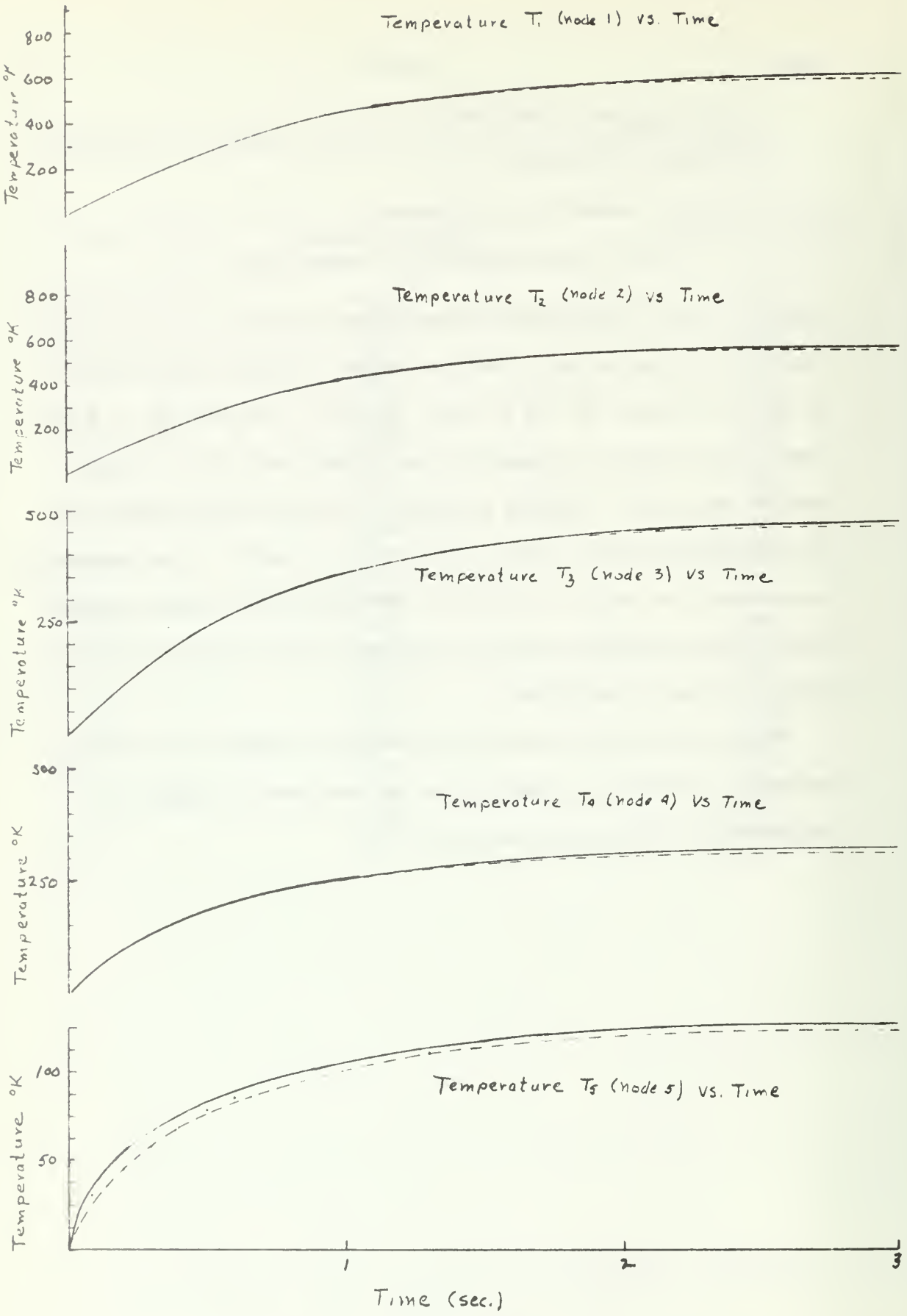

Figure 13. Comparison of Analog and Exact Solution for the Five Temperature Nodes.

V. RESULTS

The principle objective of this report was to simulate the LMFBR on the hybrid computer and to improve on the rate of convergence in the open-loop iterative method. In the development of the technique used for improving the rate of convergence it was discovered that a problem related to the stability of the converged solution existed. Because of this problem of stability of convergence (to be covered later in this section) the solution of the problem is limited to a maximum of 2 seconds.

Figure 14 and 15 show the N(t) response as a result of an external disturbance of one dollar per second which is terminated at the end of one second. The disturbance is intended to simulate the withdrawal of a control rod. The disturbance was started from a steady state operating power level of

$$S(z) = (1000 \text{ watts/cm}^2) \sin(\pi z/L).$$

L represents the length of the fuel rod which is 100 cm; z is the axial position variable. Figure 14 illustrates the process of convergence of the open-loop iterative technique. Iteration number 1 was a result of a guess for the feedback. Ten iterations were required to obtain the converged solution. Figure 15 shows the response of N(t) produced after the iteration which uses the weighting factors, and this compares favorably with the converged solution shown on the same graph.

During the development of this model it became questionable whether the open-loop iteration scheme would produce a converged

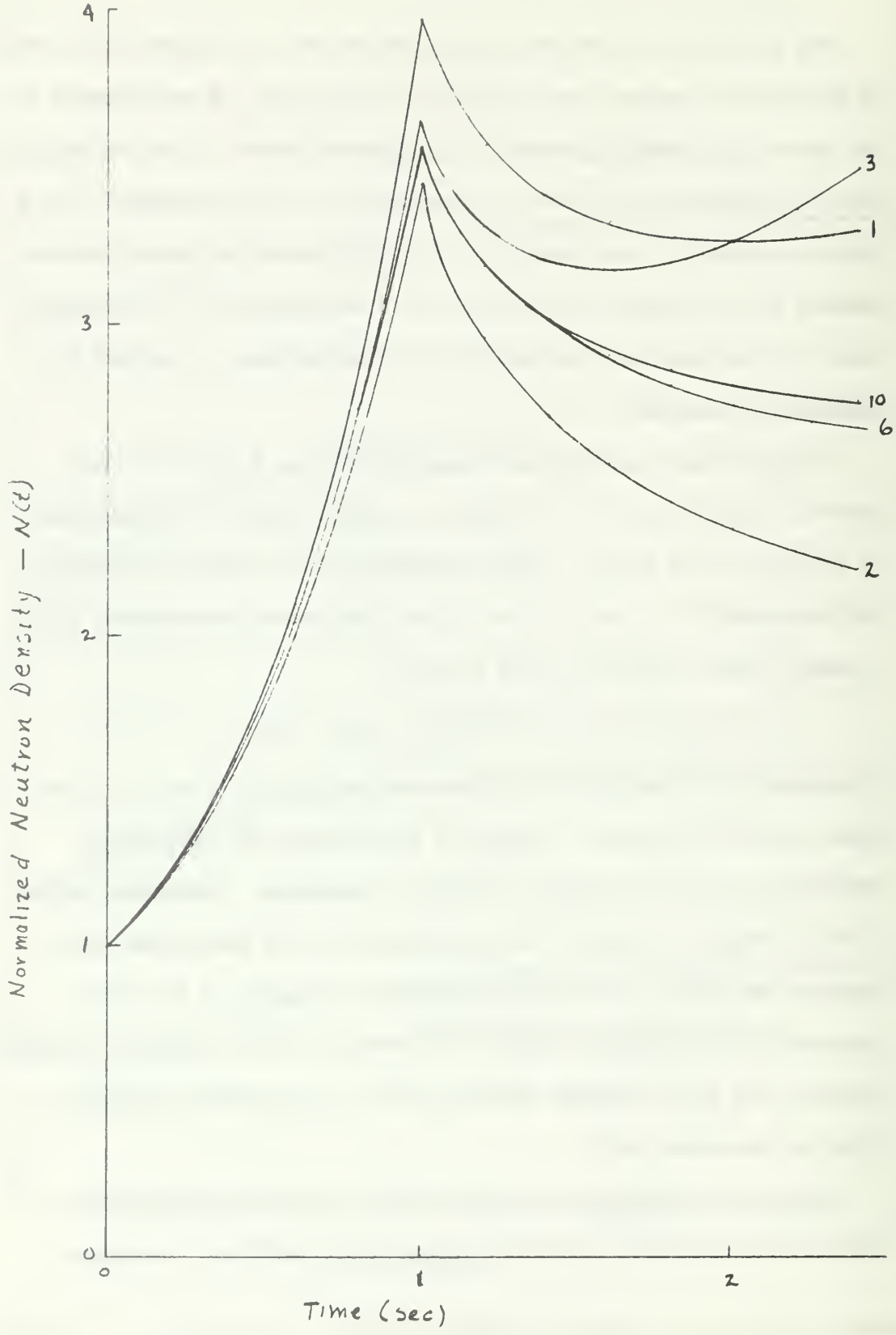

Figure 14. Illustration of Convergence Process.

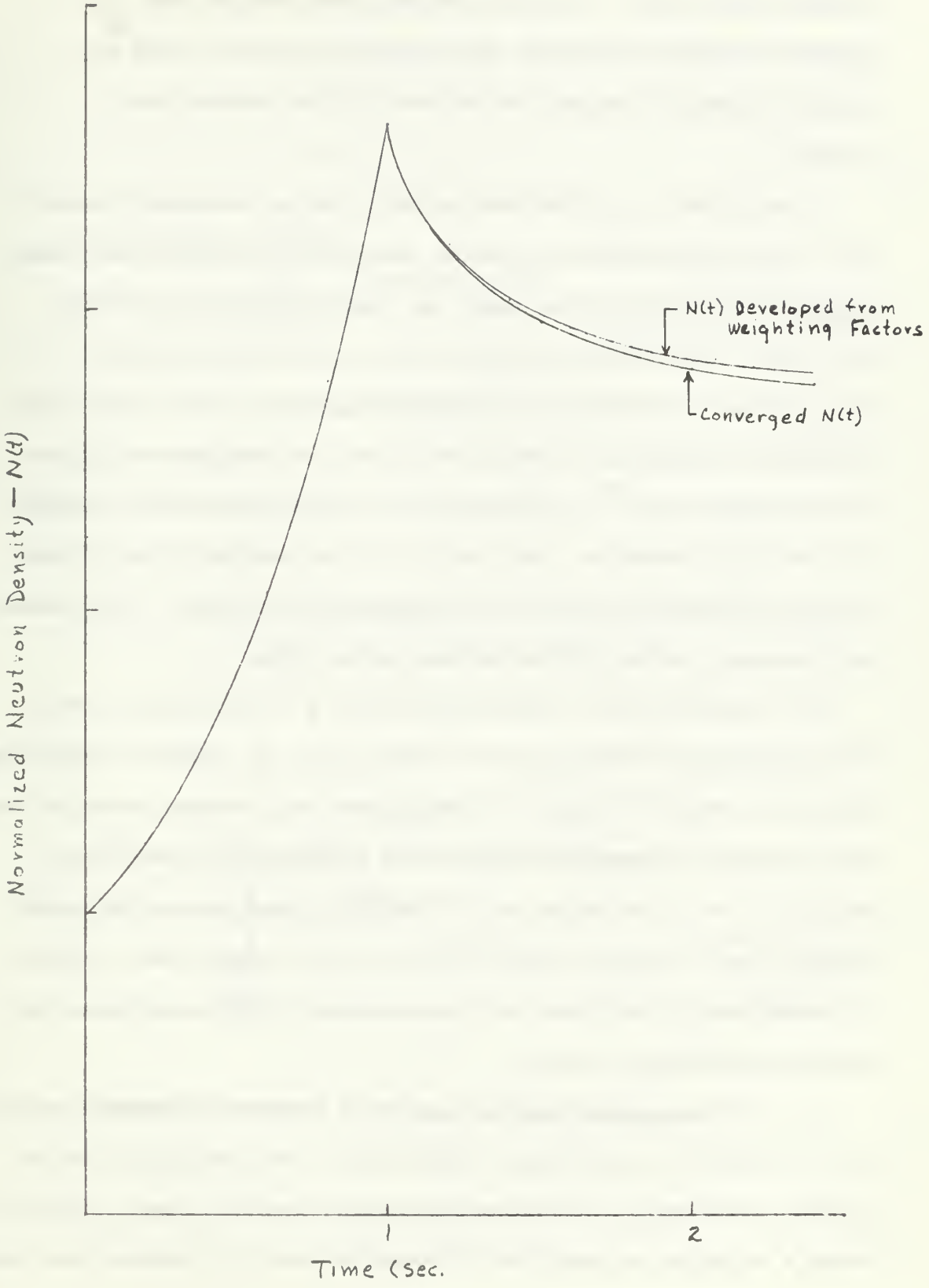

Figure 15. Comparison of Converged N(t) With N(t) Developed from Weighting Factors.

solution. Even though there exists mathematical proof that convergence occurs [Ref. 7 and 18] and published results [Ref. 7] showed the method successful, early results with this model revealed a divergent tendency for values of time greater than 2 seconds.

In an effort to isolate the problem a simple integrator circuit (Fig. 16a) was considered, since it can be shown mathematically that convergence is assured when using the open-loop iterative process [Ref. 18]. For the open-loop iterative process, the circuit in Fig. 16a can be schematically represented by that in Fig. 16b. The procedure followed was to study the behavior of the open-loop iterative process with $Y^{(1)}$ representing the closed-loop analog feedback for the first iteration. The output $Y^{(2)}$ was sampled by the digital computer and used as input for the succeeding iteration. This process was continued and the following observations made:

a) Starting with a "good solution" for $Y^{(1)}$ the behavior of E_o with successive iterations was as shown in Fig. 17 (greatly exaggerated). The region where $Y^{(2)}$ began to diverge from the converged solution was when the output approached steady state condition, or when the sum of $X + Y^{(i)} \longrightarrow 0$. The output would eventually converge but for times greater than 4 seconds (time constant for this example was 1 second) it tended more to oscillate with approximately equal error above and below the converged solution.

b) For times less than four seconds a converged solution occurred but it could not be maintained indefinitely. Periodically (with no apparent consistency) the converged solution would be lost. Figure 18 shows a converged solution and a succeeding one to illustrate this point.

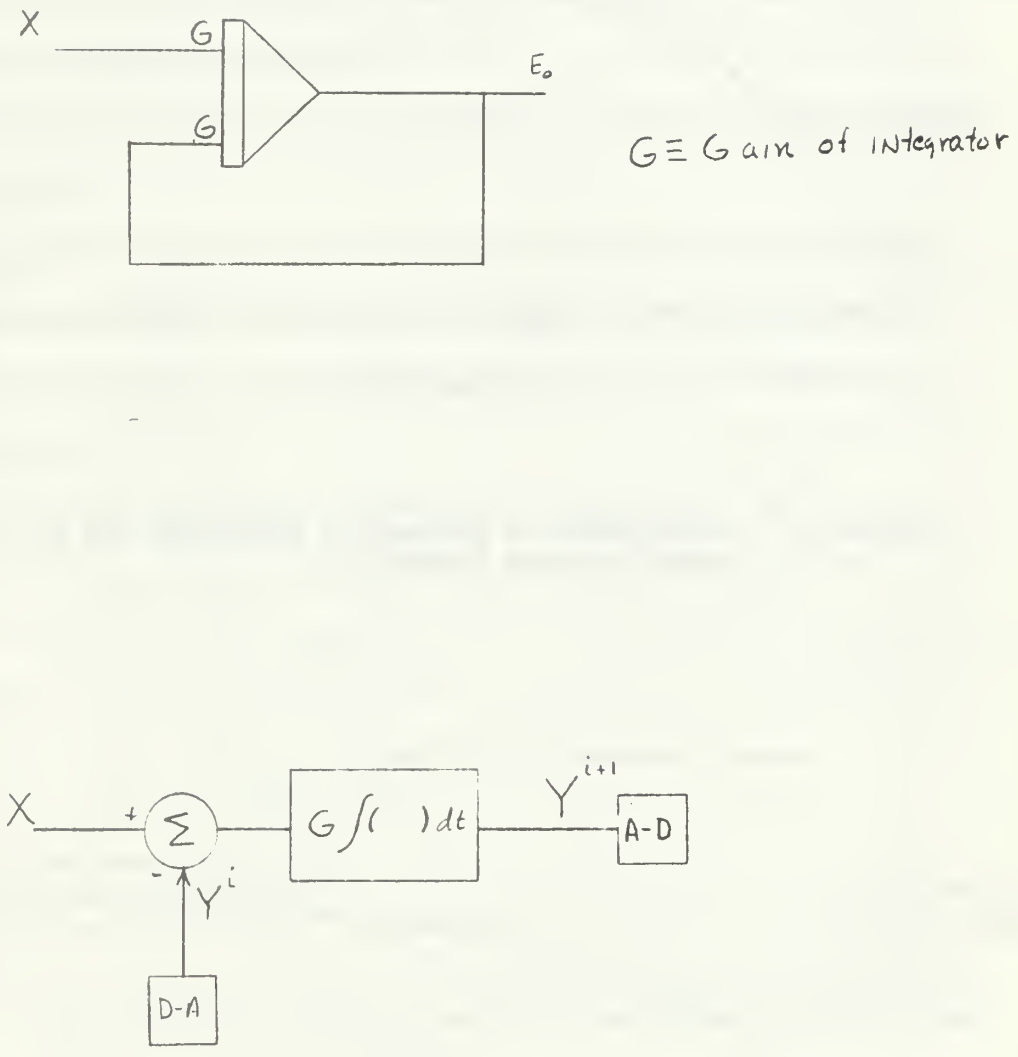

Figure 16. Diagram of Integrator with Feedback.

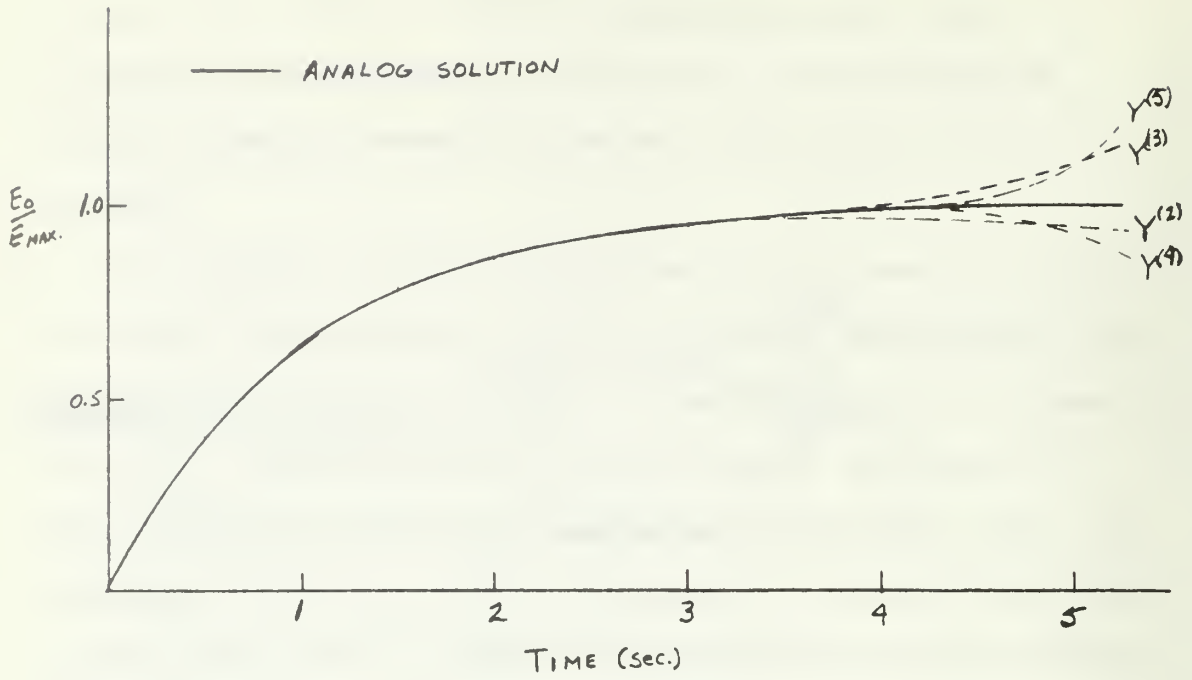

Figure 17. Illustration of Successive Iterations for Fig. 16 Using Open-Loop Method.

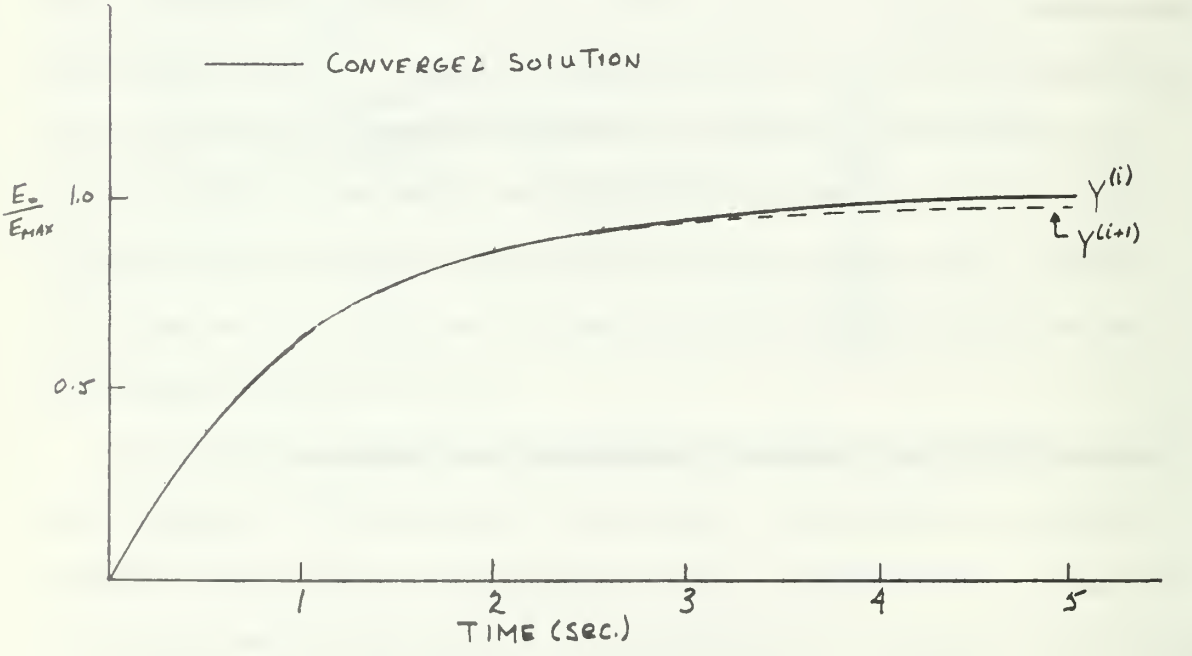

Figure 18. Illustration of Stability Problem Associated with Open-Loop Method.

The system would undergo a convergence process to again obtain a solution. Periodically (again with no apparent consistency) while in the process of converging it would lose the tendency to converge from one iteration to the next and the process would again have to repeat itself. For times up to about 3 seconds, when $X + Y^{(i)}$ was large, the output appeared unaffected and maintained a converged solution for repeated iterations.

c) The rate of convergence was slow for interval of times greater than 4 seconds.

To study the behavior of the neutron kinetics equations using the open-loop method a simple lumped-parameter model of a nuclear reactor was developed. The mathematical model for the reactor is given by equation (25).

$$\dot{N}(t) = K(t)\,N(t) + D(t) \qquad (a)$$

$$\dot{D}(t) = \lambda\,[N(t) - D(t)] \qquad (b)$$

$$\dot{\bar{T}} = a\bar{T} + A\,N(t) \qquad (c) \qquad (25)$$

$$K(t) = K_e(t) + K_f(t) \qquad (d)$$

$$K_f(t) = -\frac{A_{Dopp}}{\beta}\left(\frac{\Delta\bar{T}}{\bar{T}_o}\right) \qquad (e)$$

where, $\bar{T}$ ≡ average temperature,

$\Delta\bar{T}$ ≡ change in average temperature above $\bar{T}_o$, the initial temperature,

$1/a$ ≡ time constant of fuel. When heat is removed the temperature of fuel will fall to 1/e of its steady state value in time equal to the time constant,

A ≡ factor converting neutron density to power.

The Doppler effect was the only feedback mechanism considered and it was approximated by equation (25e); a closed-loop analog solution could then be obtained. Again the above equations can be schematically represented

as Fig. 16b. The open-loop iteration solution was attempted using the analog solution for $Y^{(1)}$. Similar behavior to the observations made above was noticed.

Two factors to be considered when using the open-loop method based on the above observations are the rate of convergence and the stability of the converged solution. The rate of convergence for the system described in Fig. 16 is slow. This can be shown as follows. If X (Fig. 16b) is considered as a step input of magnitude one, then for an initial guess of $Y^{(1)}(t) = 0$ the output, $Y^{(2)}(t)$, is equal to Gt (recalling the gain of the integrator is G). For a unit feedback the input for iteration 2 is 1 - Gt, and the output is $Gt - \frac{G^2t^2}{2}$. It is easy to show that a continued iteration process will develop the following series,

$$Y^{(i+1)} = Gt - \frac{G^2t^2}{2} + \frac{G^3t^3}{3!} - \frac{G^4t^4}{4!} + \cdots + (-1)^{i+1}\frac{G^it^i}{i!},$$

where i denotes the iteration. A necessary condition for the series to converge is $\lim_{i\to\infty} \frac{G^it^i}{i!} \to 0$. As long as G and t are finite this condition is met. However before convergence begins to occur the ratio of the i + 1 term to the i^{th} term must be less than one, or

$$\frac{Gt}{i+1} < 1 \tag{26}$$

The value of G used in Fig. 16 was 10. Thus convergence can be seen as a slow process. It is also possible to understand the initial divergent tendency of the open-loop method commented on earlier. Recalling that $Y^{(1)}$ in Fig. 17 represents the closed-loop system solution used for the first iteration, then if their exists any difference between the step input X of Fig. 16b and the feedback $Y^{(1)}$ near steady state the integrator will continue to show a change in the output with the later values of time associated with the larger

differences. If it is assumed that any difference between the analog solution and the digital solution is constant in time, it can be seen from the criteria used in developing equation (26) that the solution for early times will begin to converge while later values will tend to diverge. Eventually all times will begin to show convergence. This is illustrated by iterations 1 and 3 in Fig. 14.

There obviously exists a stability for the converged solution in the open-loop method. Since the behavior of this stability problem was not consistant nothing specific could be found that attributed to the problem. The digital to analog output was adjusted to ensure no bias voltage existed. The error between the digital and analog solution for $Y^{(1)}$ was compared and the difference was within the resolution capabilities of the equipment. The differencing of X and $Y^{(i)}$ was accomplished within the digital computer to nullify any error in the analog to digital circuit. The sampling rate at the analog to digital interface was varied from 250 to 400 Hz (400 Hz was the maximum attainable). In each case the behavior reported for Fig. 16 was observed.

The stability problem appears more pronounced when $K_e(t) + K_t(t) = K(t) \to 0$. The neutron kinetics, especially for a fast reactor with $\beta/\ell \approx 10^4$, are very sensitive to K(t) and if this quantity does not go to zero in the limit of steady state then the equations respond accordingly. It is a necessary procedure in analog simulation to ensure that with K(t) = 0 the reactor kinetics remain in the steady state condition when in the compute mode. With equation 3 which requires an integrator with a gain of $\beta/\ell \approx 10^4$ the system requires constant checking to insure a balanced condition between N and D so that the steady state solution

does not drift in the compute mode. The use of equation (5), which removes the integrator with gain β/ℓ, eliminates this need for constant checking, and it was hoped that the stability and convergence problem would be reduced. However, no noticable improvement occurred.

It can be seen from Fig. 15 that the algorithm developed in this model rapidly produces N(t) especially for times less than 1 second. However, an error exists for times greater than 1 second between the two curves and more iterations should be carried out to reach the converged curve. A converged solution is obtained in agreement with that obtained in Fig. 14, however, an unusually large number of iterations are required when compared with the rate observed in Fig. 14 in the same time region. Reference 26 reports and demonstrates that the rate of convergence is enhanced when starting from a "good initial" guess than from a "poor" one. It is suspected that the stability problem discussed earlier is effecting the rate of convergence for times greater than 1 sec. More research on this problem is needed.

VI. CONCLUSIONS AND REMARKS

The open-loop iteration process as a solution to partial differential equations is a relatively new algorithm for application on a hybrid computer. Presently only two reports [Ref. 7 and 24] have been located which present investigations into the algorithm. It is interesting to note that Ref. 24, which used the open-loop method to solve the one dimensional wave equation and heat flow equation, addressed itself to results short of the steady state solution. Also in Ref. 8, which was a follow up study on Ref. 7, the open-loop method was discarded because a large number of iterations were required near steady state conditions, and a closed-loop iteration process was adopted.

For the open-loop iteration process to be a successful tool in solving partial differential equations two problems need further investigation, namely, the rate of convergence and the stability problem observed in this report. The neutron equations can be reduced to an integral operator [Ref. 7] and therefore the convergence is slow especially for times near the steady state solution. A large number of iterations detract from the advantages of using a hybrid computer. In Ref. 24 the number of iterations in which convergence occurred over a given time interval increased substantially as the solution approached steady state.

The problem of stability near steady state solution appears to be attributed to the algorithm or the hardware. It is doubtful if the model is producing the problem since similar behavior was observed in

a very simple system, Fig. 16. Further investigation is needed to establish the source of this problem. It is suggested that based on the investigation carried out in this report that the problem is inherent with the open-loop method.

One possibility looks encouraging for future studies in solving the rate of convergence and the stability problem. The technique employed in Ref. 8 utilizes a closed-loop iteration process. The method rapidly develops N(t) for later values of time but N(t) for intermediate values of time required more iterations. The algorithm in this report develops N(t) for early times but requires additional iterations to reach a solution. A combination of the two may prove fruitful.

In addition the use of the Diode Function Generator represents a very flexible tool when used to duplicate a nonlinear function. This is especially demonstrated when incorporated in the continuous solution to the nonlinear heat flow equation. The procedure used in Ref. 7 was to approximate K(T) as a third order polynomial which resulted in the need for a large number of multipliers and summer amplifiers. Also the DFG can approximate the curve more accurately then can the third order polynomial.

It is also worthwhile to note that the present hybrid simulation has the following limitations:

1) The bonding between the fuel and cladding was neglected. This will produce lower temperatures in the fuel than actually encountered. An attempt was made to include the bonding but the analog circuit was unstable.

2) The point model neutron kinetics are used to describe the behavior of the entire core.

3) Axial flow of heat is neglected. This will result in producing higher temperatures. However any error in temperature introduced here is considered negligible.

4) The assumption that an average fuel cell gives all the information necessary to obtain the average core temperature may lead to unrealistic dynamic behavior [Ref. 6]. However in the design of the General Electric LMFBR the fissile fuel is varied radially within the core to flatten the power flux. This would tend to make the assumption more realistic.

Presently this model is very complex and some problems with the present model need further investigation before the limitations outlined above can be considered.

APPENDIX A

A. MATHEMATICAL PROOFS AND DERIVATIONS

1. Kinetic Equations

The kinetic equations are recast here in the reduced variable form. Equation (1) is considered with one precursor concentration, namely,

$$\frac{dn(t)}{dt} = \frac{1}{\ell}\left[\rho(t) - \beta\right] n(t) + \lambda\, c(t) \qquad (a)$$

$$\frac{dc(t)}{dt} = \frac{\beta}{\ell}\, n(t) - \lambda\, c(t) \qquad (b) \qquad (1)$$

where, $\lambda = \dfrac{\sum_{i=1}^{6} \beta_i \lambda_i}{\sum_{i=1}^{6} \lambda_i}$.

Equation (1a) is divided by $n(0)$ and equation (1b) by $c(0)$, which are the values of neutron and precursor concentration (#/cm^3) respectively at steady state. Defining two quantities, $N(t) = \frac{n(t)}{n(0)}$ and $D(t) = \frac{c(t)}{c(0)}$ equation (1) becomes

$$\frac{dN(t)}{dt} = \frac{1}{\ell}\left[\rho(t) - \beta\right] N(t) + \lambda\, \frac{c(t)}{n(0)} \qquad (a)$$

$$\frac{dD(t)}{dt} = \frac{\beta}{\ell}\, \frac{n(t)}{c(0)} - \lambda\, D(t) \qquad (b) \qquad (27)$$

At steady state $\frac{dn(t)}{dt} = \frac{dc(t)}{dt} = 0$ in equation (1), therefore, $\frac{\beta}{\ell}\, n(0) = \lambda\, c(0)$. Putting this into equation (27) the following equations are obtained,

$$\frac{dN(t)}{dt} = \frac{1}{\ell}\left[\rho(t) - \beta\right]N(t) + \frac{\beta}{\ell} D(t) \qquad (a)$$

$$= \frac{\beta}{\ell}\left[\frac{\rho(t)}{\beta} N(t) - N(t) + D(t)\right] \qquad (28)$$

$$\frac{dD(t)}{dt} = \lambda\left[N(t) - D(t)\right] \qquad (b)$$

The quantity $\rho(t)/\beta \equiv K(t)$ has the units of dollars. Thus one dollars worth of reactivity indicates ρ (the excess reactivity) has the value of β . Introducing the term K(t) equation (2) is obtained.

$$\frac{dN(t)}{dt} = \frac{\beta}{\ell}\left[K(t)N(t) - N(t) + D(t)\right] \qquad (a)$$

$$\frac{dD(t)}{dt} = \lambda\left[N(t) - D(t)\right] \qquad (b) \qquad (2)$$

where at t = 0, N(0) = D(0) = 1.

2. Reactivity Feedback

a. Doppler Effect

In a LMFBR the Doppler effect contributes the majority of the feedback [Ref. 9]. A highly simplified picture [Ref. 25] of the Doppler effect is illustrated in Fig. 19. The cross-section curve which shows the probability of a nucleus-neutron reaction is shown at left. At the right (Case I) is a picture of a neutron approaching a nucleus at a low temperature. Since the nucleus is essentially at rest neutrons with a lesser or greater velocity than that occurring at resonance will escape the reaction. However as the temperature increases (Case II) the nucleus is no longer at rest and neutrons of lower or higher velocity can still achieve the same relative velocity. The effect is to broaden the resonance peak and increase the chances of a neutron being absorbed. The absorption of neutrons for other than fission processes dominates and a negative reactivity occurs.

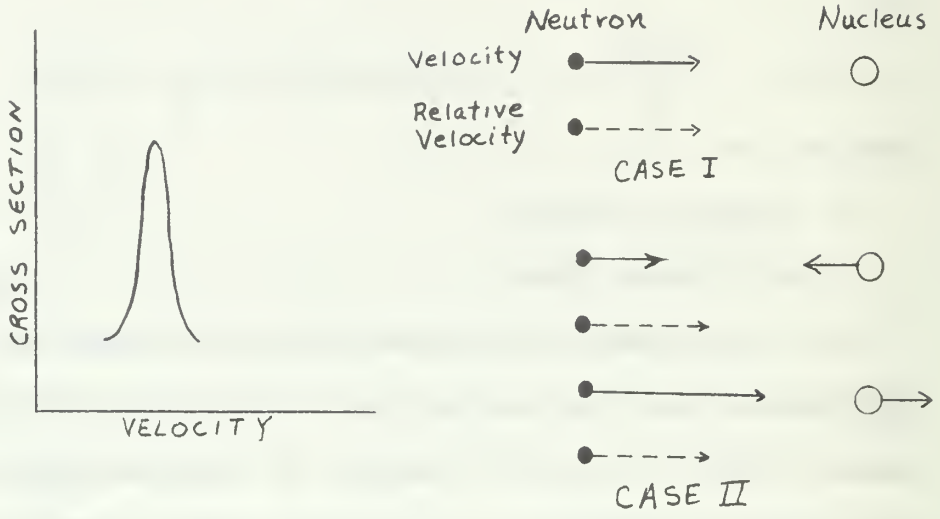

Figure 19. Illustration of Dopper Effect.

A development of an exact mathematical model for the Doppler effect has been hampered due to lack of experimental data for neutron cross sections at higher energies. It is necessary to use statistical treatments [Ref. 26] which yield for the Doppler effect the expression:

$$\frac{\partial \rho}{\partial T} \propto T^{-3/2}$$

However recent results by R. Froelich, and others [Ref. 27] indicate the Doppler effect to be

$$\frac{\partial \rho}{\partial T} = -C\left(\frac{300}{T}\right)^{\gamma}$$

where C and γ are positive constants depending on volume ratio of UO_2 to PO_2 and sodium density. γ is approximately equal to one. In the General Electric reactor under design γ is equal to one. Therefore the Doppler effect is:

$$\frac{\partial \rho}{\partial T} = -\frac{A_{Dopp}}{\bar{T}}$$

where $\bar{T}$ is the average temperature of the core and A_{Dopp} is a position constant termed the Doppler coefficient. Starting at an average temperature of the core, $\bar{T}_o$, the change in reactivity due to Doppler effect (ρ_{Dopp}) can be expressed as follows:

$$\rho_{Dopp} = -A_{Dopp}\int_{\bar{T}_o}^{\bar{T}} \frac{d\bar{T}}{\bar{T}} = -A_{Dopp}\ln\left(1+\frac{\Delta\bar{T}}{\bar{T}_o}\right)$$

or, in terms of dollars

$$K_{Dopp} = \frac{-A_{Dopp}}{\beta}\ln\left(1+\frac{\Delta\bar{T}}{\bar{T}_o}\right)$$

b. Fuel Expansion

The expansion of the fuel gives rise to a negative feedback. It can be explained somewhat simply by observing that an expansion of the fuel reduces the fission nuclei per cm^2 seen by the flux of neutrons. In the General Electric design LMFBR it is expressed as

$$\rho_{exp} = - B_{exp} \Delta \bar{T}_f$$

or, in dollar units

$$K_{exp} = - \frac{B_{exp}}{\beta} \Delta \bar{T}_f$$

where B_{exp} is a positive constant.

c. Coolant Expansion

The expansion of the coolant can give rise to either a positive or negative feedback. As the coolant expands the number of neutrons captured parasitically is reduced thereby increasing reactivity. Changes occur in neutron leakage (loss of scattering events by sodium) when the coolant expands and, hence, reduction of reactivity occurs. Also less moderation occurs producing a hardening of the neutron spectrum, and if fertile materials are present more fissions occur producing an increase in reactivity. The size of the core, fuel and volume ratio of coolant determine which of the above are more pronounced. In the General Electric reactor the feedback due to coolant expansion is positive and expressed as follows,

$$\rho_{cool} = C_{cool} \Delta \bar{T}_c$$

or, in dollar units,

$$K_{cool} = C_{cool} \Delta \bar{T}_c / \beta$$

where C_{cool} is a positive constant usually referred to as the sodium void coefficient.

3. Heat Flow Equations

From Section IIA the equation for heat flow in the fuel rod is,

$$c_f d_f \frac{\partial T}{\partial t} = \frac{1}{r} \frac{\partial}{\partial r} \left[K_f(T) r \frac{\partial T}{\partial r} \right] + S(z) N(t) \qquad (9)$$

Figure 20 illustrates the various radial segments selected within the fuel pin. The temperature between mid-points of each radial segment is assumed to vary linearly. The slope at each side of a segment interface are equal thus ensuring that the flow of heat across the boundary is continuous. Applying equation (8) to the region indicated in Fig. 20 and integrating over the spacial variable r the following equation is obtained,[5]

$$\int_{r_i-\frac{\Delta r}{2}}^{r_i+\frac{\Delta r}{2}} r c_f d_f \frac{\partial T}{\partial t}\, dr = \int_{r_i-\frac{\Delta r}{2}}^{r_i+\frac{\Delta r}{2}} \frac{\partial}{\partial r}\left[K_f(T)\, r \frac{\partial T}{\partial r}\right] dr + \int_{r_i-\frac{\Delta r}{2}}^{r_i+\frac{\Delta r}{2}} r\, s(z)\, N(t)\, dr$$

For clarity each integral will be handled separately. Assuming K(T) is not a constant, the first expression on the right side becomes,

$$\int_{r_i-\frac{\Delta r}{2}}^{r_i+\frac{\Delta r}{2}} \frac{\partial}{\partial r}\left[K_f(T)\, r \frac{\partial T}{\partial r}\right] dr = \left[K(T)\, r \frac{\partial T}{\partial r}\right]_{r_i-\frac{\Delta r}{2}}^{r_i+\frac{\Delta r}{2}}$$

$$= K_{f,i+1,i}\left(r_i+\frac{\Delta r}{2}\right)\left(\frac{T_{i+1}-T_i}{\Delta r}\right) \qquad (29)$$

$$-K_{f,i,i-1}\left(r_i-\frac{\Delta r}{2}\right)\left(\frac{T_i-T_{i-1}}{\Delta r}\right)$$

where, $K_{f,i+1,i}$ = thermal conductivity at the boundary between node i + 1 and i. The temperature at the boundary is $\frac{T_{i+1}+T_i}{2}$

The second integral on the right side reduces to,

---

[5]Reference 15 states this technique of reducing a partial differential equation to an ordinary differention equation requires a minimum number of nodes.

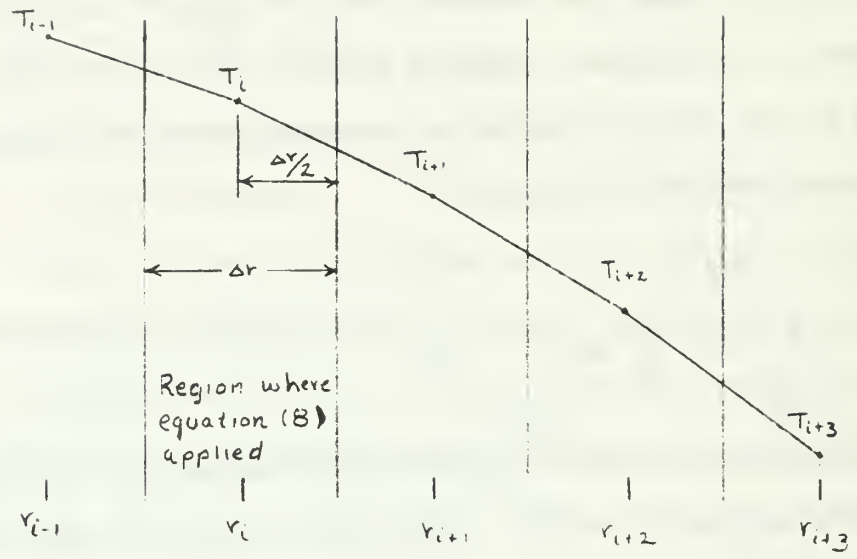

Figure 20. Temperature Profile Within Fuel.

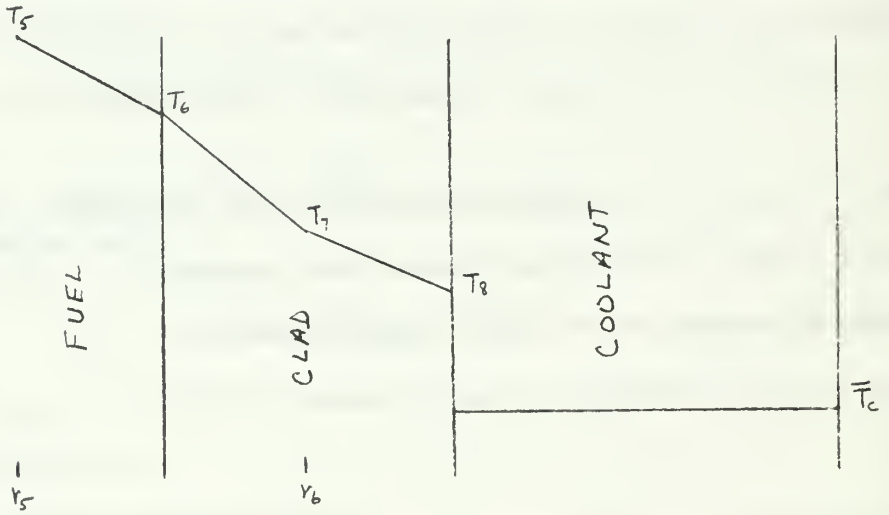

Figure 21. Temperature Profile Within Cladding and Coolant.

$$\int_{r_i-\frac{\Delta r}{2}}^{r+\frac{\Delta r}{2}} r\, s(z)\, N(t)\, dr = s(z)\, N(t) \int_{r_i-\frac{\Delta r}{2}}^{r_i+\frac{\Delta r}{2}} \frac{r^2}{2} \tag{30}$$

$$= s(z)\, N(t)\, r_i\, \Delta r$$

The quantity $c_f d_f$ in the integral on the left hand side of equation (9) is assumed to be a constant[6], therefore, $c_f d_f$ and the operator $\partial/\partial t$ can be brought outside the integral. The integral is then handled as follows:

$$\int_{r_i-\frac{\Delta r}{2}}^{r_i+\frac{\Delta r}{2}} r\, c_f d_f \frac{\partial T}{\partial t}\, dr = c_f d_f \frac{\partial}{\partial t}\left[\int_{r_i-\frac{\Delta r}{2}}^{r_i+\frac{\Delta r}{2}} r\, T\, dr\right] \tag{31}$$

From Fig. 20 the relation for T is,

$$T = \begin{cases} T_{i-1} - \left(\frac{T_{i-1} - T_i}{\Delta r}\right)\left(r - r_i + \frac{\Delta r}{2}\right), & \left(r_i - \frac{\Delta r}{2}\right) \le r \le r_i \\ T_i - \left(\frac{T_i - T_{i+1}}{\Delta r}\right)\left(r - r_i\right), & r_i < r \le \left(r_i + \frac{\Delta r}{2}\right) \end{cases}$$

Therefore equation (31) becomes,

$$c_f d_f \frac{\partial}{\partial t}\left\{\int_{r_i-\frac{\Delta r}{2}}^{r_i} r\left[T_{i-1} - \left(\frac{T_{i-1} - T_i}{\Delta r}\right)\left(r - r_i + \frac{\Delta r}{2}\right)\right] dr\right.$$

$$\left. + \int_{r_i}^{r_i+\frac{\Delta r}{2}} r\left[T_i - \left(\frac{T_i - T_{i-1}}{\Delta r}\right)\left(r - r_i\right)\right] dr\right\}$$

---

[6] In most materials this can be considered a constant and in UO_2 the variation is not pronounced. Reference 15 treats the condition where $c_f d_f$ is not a constant.

$$= C_f d_f \frac{\partial}{\partial t} \left\{ \left[T_{i-1} \frac{r^2}{2} - \left(\frac{T_{i-1} - T_i}{\Delta r} \right) \left(\frac{r^3}{3} - \frac{r_i r^2}{2} + \frac{\Delta r}{4} r^2 \right) \right]_{r_i - \frac{\Delta r}{2}}^{r_i} \right.$$

$$\left. + \left[\frac{T_i r^2}{2} - \left(\frac{T_i - T_{i-1}}{\Delta r} \right) \left(\frac{r^3}{3} - \frac{r_i r^2}{2} \right) \right]_{r_i}^{r_i + \frac{\Delta r}{2}} \right\} \tag{32}$$

After applying limits and some reduction equation (32) becomes:

$$= C_f d_f \frac{\partial}{\partial t} \left[T_{i+1} \left(\frac{1}{8} r_i \Delta r + \frac{\Delta r^2}{24} \right) + \frac{3}{4} T_i \Delta r r_i \right.$$

$$\left. + T_{i-1} \left(\frac{1}{8} \Delta r r_i - \frac{\Delta r^2}{24} \right) \right] \tag{33}$$

The operator $\partial/\partial t$ in equation (33) can be changed to $\frac{d}{dt}$ since the space variable has been eliminated. Combining equations (29), (30), and (33) and after dividing through by $r_i \Delta r$ the following equation is obtained,

$$C_f d_f \frac{d}{dt} \left[T_{i+1} \left(\frac{1}{8} - \frac{\Delta r}{24 r_i} \right) + \frac{3}{4} T_i + T_{i-1} \left(\frac{1}{8} - \frac{\Delta r}{24 r_i} \right) \right]$$

$$= K_{f,i,i+1,i} \left(1 + \frac{\Delta r}{2 r_i} \right) \left(\frac{T_{i+1} - T_i}{\Delta r^2} \right) - K_{f,i,i-1} \left(1 - \frac{\Delta r}{2 r_i} \right) \left(\frac{T_i - T_{i-1}}{\Delta r^2} \right) \tag{34}$$

$$+ S(z) N(t)$$

The equation for heat flow in the cladding is,

$$c_c d_c \frac{\partial T}{\partial t} = \frac{1}{r} \frac{\partial}{\partial r} \left[K_c(T) r \frac{\partial T}{\partial r} \right] \tag{10}$$

For the cladding which for this model is stainless steel the quantities $c_c d_c$ and K_c are assumed constant. Following an identical procedure as above and utilizing Fig. 21 equation (10) can be reduced to,

$$c_c d_c \frac{d}{dt}\left[T_6\left(\frac{1}{4} - \frac{\Delta r_c}{12 r_6}\right) + \frac{T_7}{2} + T_8\left(\frac{1}{8} + \frac{\Delta r_c}{12 r_6}\right)\right]$$

$$= K_c\left(1 + \frac{\Delta r_c}{2 r_6}\right)\left(\frac{T_6 - T_7}{\Delta r_c^2/2}\right) - K_c\left(1 - \frac{\Delta r_c}{2 r_6}\right)\left(\frac{T_7 - T_8}{\Delta r^2/2}\right) \qquad (35)$$

To differentiate one axial segment from the next, superscript j is used and equations (34) and (35) become equations (11) and (12) used in Section IIB.

To the clad-coolant interface the conservation of energy is applied to develop a differential equation which couples each axial segment. As stated earlier the axial flow of heat is neglected and therefore no coupling of one axial segment with its neighbor exists within the fuel and cladding regions. The coupling occurs through the flowing coolant.

Figure 22 represents a top and side view of an axial segment. If the coolant is treated as a heat sink, the temperature drops at the clad-coolant interface to a value assumed constant (Fig. 21) over the region which receives heat from the segment in question. Δr_{cool} represents the extent in the radially direction of this region. The radial gradient of temperature in coolant is neglected.

The heat (δq) received by the coolant is

$$\delta q = 2\pi r_c (\Delta z)(\Delta r_{cool}) c_{cool} d_{cool} dT_c(t,z) \qquad (36)$$

$$\text{but, } dT_c(t,z) = \frac{\partial T_c}{\partial z} dz + \frac{\partial T_c}{\partial t} dt$$

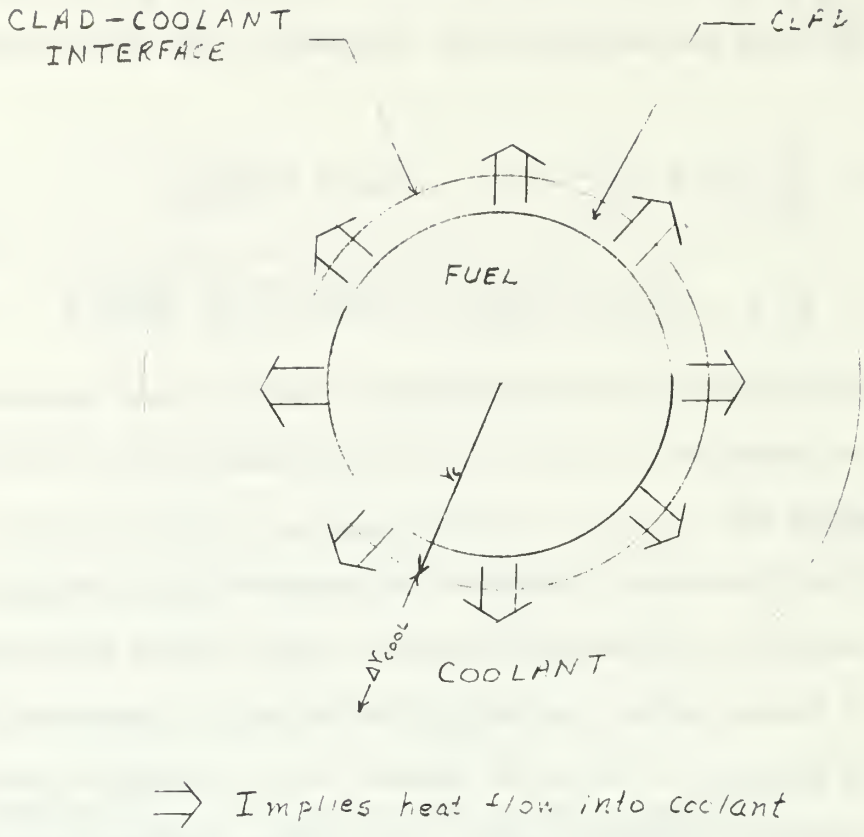

Figure 22. Diagram of Axial Segment.

therefore equation (36) becomes

$$\frac{dq}{2\pi r_c \Delta z \Delta r_{cool}} = d_c c_c \left[\frac{\partial T_c}{\partial z} dz + \frac{\partial T_c}{\partial t} dt \right] \tag{37}$$

or,

$$\frac{1}{\Delta r_{cool}} \frac{dq}{2\pi r_c \Delta z \, dt} \frac{1}{c_{cool} d_{cool}} = \frac{\partial T_c}{\partial z} \left(\frac{d_{cool} \frac{dz}{dt}}{d_{cool}} \right) + \frac{\partial T_c}{\partial t} \tag{38}$$

$d_{cool} \frac{dz}{dt}$ = Mass flow rate of coolant $\equiv G(t)$

$\frac{dq}{2\pi r_c \Delta z \, dt}$ = Heat flux across clad-coolant interface $\equiv H$

Both numerator and denominator of the left side of equation (39) are now multiplied by $2\pi r_c$ in order to cast it in a form to take advantage of certain design criteria. In a reactor the volume fraction of coolant is a known design criteria and this knowledge allows the evaluation of $2\pi r_c \Delta r_{cool}$, which is approximately the cross section of coolant. In most LMFBR designs [Ref. 28] considered to date, including the General Electric model used herein, the volume fraction of coolant $\approx 50\%$ implying the cross section of coolant equals the combined cross section of fuel and clad. Therefore,

$\frac{2\pi r_c}{2\pi r_c \Delta r_{cool}}$ = ratio of circumference of clad to cross sectional area of coolant

$$= \frac{2\pi r_c}{\pi r_c^2} = \frac{2}{r_c}$$

Equation (38) may now be written as,

$$\frac{G(t)}{d_{cool}} \frac{\partial T_c}{\partial z} + \frac{\partial T_c}{\partial t} = \frac{2H}{d_{cool} c_{cool} r_c} \tag{39}$$

Again an ordinary differential equation is sought in order to use the analog computer. To reduce equation (39) to an ordinary differential equation the finite differencing technique [Ref. 29] is employed by discretizing the space variable. The operator $\partial/\partial z$ is reduced to $\frac{T_c^j - T_c^{j-1}}{\Delta z}$. Also, a linear relationship is assumed for T_c across the Δz segment, thus, the average coolant temperature ($\bar{T}_c$) for a segment can be expressed as

$$\bar{T}_c^j = \frac{T_c^j + T_c^{j-1}}{2}$$

$j = 1, 2, 3 \cdots\cdots 10$ (10 being the number of segments)

Ten axial segments were found adequate to describe the coolant temperature profile in agreement with Ref. 7. T_c^{j-1} represents the outlet temperature from the previous segment and T_c^j the outlet temperature of the segment in question.

With these substitutions equation (40) becomes,

$$\frac{d\bar{T}_c^j}{dt} + \frac{G(t)}{d_{cool}} \left(\frac{T_c^j - T_c^{j-1}}{\Delta z} \right) = \frac{2H}{c_{cool}\, d_{cool}\, \gamma_c}$$

but, $T_c^j = 2\bar{T}^j - T_c^{j-1}$

therefore,

$$\frac{d\bar{T}_c^j}{dt} + \frac{2G(t)}{\Delta z\, d_{cool}} \left(\bar{T}_c^j - T_c^{j-1} \right) = \frac{2H}{d_{cool}\, c_{cool}\, \gamma_c} \qquad (14)$$

APPENDIX B

A. SCALING OF DIFFERENTIAL EQUATIONS

The scaling of the differential equations (15) through (21) will be demonstrated by using equation (15)

$$\frac{d}{dt}\left[T_1' + .2633\,T_2^i\right] = 328.2\left[K_{f,1,2}\left(T_2^i - T_1^i\right)\right] + .4100\,S(z)\,N(t) \quad (15)$$

The various quantities (T_1, T_2, $K_{f/2}$ etc.) are represented on the analog computer as voltages whereas in equation (15) they represent units (^{o}K, watts/cm^3, etc.), therefore a coefficient called a scaling factor is needed which transforms the various units into voltages. Thus the following expression for each variable in equation (1) is defined.

$$T_1 \equiv k_T \bar{T}_1$$

$$T_2 \equiv k_T \bar{T}_2$$

$$K_{f,1,2} \equiv k_K \bar{K}_{f,1,2}$$

$$N(t) \equiv k_N \bar{N}(t)$$

$$S(z) \equiv k_S \bar{S}(z)$$

where $\bar{T}_1$, $\bar{T}_2$, $\bar{K}_{f/2}$ $\bar{N}(t)$ and $\bar{S}(z)$ are in volts. Placing these quantities into equation (15) and dividing through by k_T gives

$$\frac{d}{dt}\left[\bar{T}_1^i + .2633\,\bar{T}_2^i\right] = 328.2\left[k_K\,\bar{K}_{f,1,2}\left(\bar{T}_2^i - \bar{T}_1^i\right)\right] + .41\left(\frac{k_N k_S}{k_T}\right)\bar{S}(z)\,\bar{N}(t) \quad (40)$$

The value of the scaling factors k_T, k_K, k_s and k_N are determined by knowing the maximum voltages the variables will assume during the

solution. These are sometimes not known and often the problem must be put on the computer and tested before arriving at scaling factors. In this case it was found convenient to use the following values for the scaling factors,

$$k_T = 20\ ^{\circ}K/Volt$$

$$k_K = 1\ \frac{Watts}{cm\text{-}^{\circ}C\text{-}Volt}$$

$$k_S = 100\ \frac{Watts}{cm^3\text{-}Volt}$$

$$k_N = .1/Volt$$

With these scaling factors equation (40) becomes

$$\frac{d}{dt}\left[\bar{T}_1^j + .2633\bar{T}_2^j\right] = 32.82\left[10\,\bar{K}_{t,2,1}\left(\bar{T}_2^j - \bar{T}_1^j\right)\right] + .205\,\bar{S}(z)\bar{N}(t) \quad (41)$$

Similar operation on the remaining equations (16) through (21) produce the following equations

$$\frac{d}{dt}\left[\bar{T}_2^j + .2038\bar{T}_3^j + .1295\bar{T}_1^j\right] = 23.1\left[10\,\bar{K}_{t,3,2}\left(\bar{T}_3^j - \bar{T}_2^j\right)\right] - 11.55\left[10\,\bar{K}_{t,2,1}\left(\bar{T}_2^j - \bar{T}_1^j\right)\right] + .2165\,\bar{S}(z)\,\bar{N}(t) \quad (42)$$

$$\frac{d}{dt}\left[\bar{T}_3^j + .1889\,\bar{T}_4^j + .1444\bar{T}_2^j\right] = 20.8\left[10\,\bar{K}_{t,4,3}\left(\bar{T}_4^j - \bar{T}_3^j\right)\right] - 13.88\left[10\,\bar{K}_{t,3,2}\left(\bar{T}_3^j - \bar{T}_2^j\right)\right] + .2165\,\bar{S}(z)\,\bar{N}(t) \quad (43)$$

$$\frac{d}{dt}\left[\bar{T}_4^j + .1826\bar{T}_5^j + .1507\bar{T}_3^j\right] = 19.81\left[10\bar{K}_{t,5,4}\left(\bar{T}_5^j - \bar{T}_4^j\right)\right] - 14.85\left[10\,\bar{K}_{t,4,3}\left(\bar{T}_4^j - \bar{T}_3^j\right)\right] + .2165\,\bar{S}(z)\,\bar{N}(t) \quad (44)$$

$$\frac{d}{dt}\left[\bar{T}_5^j + .1890\,\bar{T}_4^j + .4362\,\bar{T}_6^j\right] = 46.9\left[10\,\bar{K}_{t,6}\left(\bar{T}_6^j - \bar{T}_5^j\right)\right] - 18.75\left[10\,\bar{K}_{t,5,4}\left(\bar{T}_5^j - \bar{T}_4^j\right)\right] + .264\,\bar{S}(z)\,\bar{N}(t) \quad (45)$$

$$\frac{d}{dt}\left[\bar{T}_8^j + 1.885\bar{T}_7^j + .885\bar{T}_6^j\right] = 174.1\left[\bar{T}_2^j - \bar{T}_7^j\right] - 69.8\left[10\,R_{f,6}\left(\bar{T}_6^j - \bar{T}_5^j\right)\right] \tag{46}$$

$$\frac{d}{dt}\bar{\bar{T}}_c^j = -456.3\,\bar{\bar{T}}_c^j + 118.8\,\bar{T}_8^j + 337.5\,\bar{T}_c^{j-1} \tag{47}$$

(Note: $\bar{\bar{T}}_c^{\,j}$ refers to average coolant temperature in volts)

APPENDIX C

A. PHYSICAL PARAMETERS[7]

Specific heat-c (watt-sec/gm-^{o}C

Fuel - 0.3345

Cladding- 0.502

Coolant - 0.21

Thermal conductivity-K(T) (watts/cm-^{o}C

Fuel - see Fig. 5

Cladding - 0.2075

Density-ρ (gm/cm^{3})

Fuel - 9.2

Cladding - 8.0

Coolant - 0.8

Mass flow rate of coolant-G(t) (gm/cm^{2}-sec

500

Heat transfer coefficient between clad and coolant-h (watts/cm^{2}-^{o}C

13.08

Dimensions (cm)

$\Delta r = 0.05$

$\Delta r_c = 0.05$

$\Delta z = 10$

$L = 100$

Prompt neutron lifetime-ℓ (sec)

4.8×10^{-7}

---

[7]Values taken from Ref. 9 and personal correspondence with Mr. C. K. Sanathanan.

Decay constant for six precursor model-$\lambda i (sec^{-1})$

i	λi
1	0.0130
2	0.0314
3	0.136
4	0.340
5	1.320
6	3.500

Delayed neutron fraction from i^{th} group-βi

i	βi
1	.0000759
2	.000626
3	.000564
4	.0010700
5	.000489
6	.000163

$$\beta = \sum_{i=1}^{6} \beta_i = .002988$$

Decay constant for one precursor model-$\lambda (sec^{-1})$

$$\lambda = \frac{\sum_{i=1}^{6} \lambda_i \beta_i}{\sum_{i=1}^{6} \beta_i} = .5808$$

$A_{Dopp} = 0.005$

$B_{exp} = 3 \times 10^{-7}$

$C_{cool} = 2 \times 10^{-6}$

BIBLIOGRAPHY

1. Atomic Energy Commission Res. and Dev. Report WASH - 1101 (TID - 4500, UC80), Liquid Metal Fast Breeder Reactor Program Plan - Vol. 1, by LMFBR Program Office, Argonne National Laboratory, Aug. 1968.

2. Beekman, M. C., Incentives for Development of Fast Breeder Reactor Power Plants, Proceedings of the National Topical Meeting on Fast Reactor Systems, Materials and Components, CONF - 680419, p. 9, April 2-4, 1968.

3. Goldsmith, S., Jackson, R. J., and Weber, E. T., Ceramic Fuels for Fast Reactors, Proceedings of the National Topical Meeting on Fast Reactor Systems, Materials and Components, CONF - 680419, p. 165, April 2-4, 1968.

4. Dickinson, R. W., LMFBR System and Component Test Facilities, Proceedings of the National Topical Meeting on Fast Reactor Systems, Materials and Components, CONF - 680419, p. 422, April 2-4, 1968.

5. Blake, R., and others, Hybrid Computer Optimization of a Nuclear Power Station Control System, Proceedings Internation Symposium on an Analog/Hybrid Computation Applied to Nuclear Energy, Versailles, Sept. 16-18, 1968.

6. Carlson, A. M., Hybrid Simulation of an Exchange - Reactor Control System, Technical Conference on Process Control (Sponsored by N.R.C.), Edmonton, Alberta, Canada, May, 1968.

7. Sanathanan, C. K., and others, Hybrid Computers in the Analysis of Feedback Control Systems, Proceedings of the Fall Joint Computer Conference, Vol. 29, p. 743, Nov. 1966.

8. Sanathanan, C. K., and others, Advances in the Hybrid Simulation of Nuclear Reactor Transients, Proceedings International Symposium on Analog/Hybrid Computation Applied to Nuclear Energy, Versailles, France, Sept. 16-18, 1968.

9. General Electric Atomic Power Equipment Department, San Jose, Calif., GEAP - 4418 (1964), Liquid Metal Fast Breeder Reactor Design Study (1000 MWe UO_2 - PUO_2 Fueled Plant), by M. J. McNelly.

10. Henry, A. F., "The Application of Reactor Kinetics to the Analysis of Experiments", Nuc. Sci. and Eng., v. 3, p. 52, 1958.

11. Gyftopoulos, E. P., Point Reactor Kinetics and Stability Criteria, Third United Nations International Conference on the Peaceful Uses of Atomic Energy, Geneva, p. 270, May 1964.

12. Jakeman, D., Physics of Nuclear Reactors, American Elsevier Publishing Co., Inc.

13. MacFarlane, D. R., and others, "Sodium Boiling Transients in Oxide - Fueled Fast Reactors", Nuc. Sci. and Eng., v. 7, p. 411, May, 1968.

14. General Electric Atomic Power Equipment Department, San Jose, Calif., GEAP - 4090 (Oct. 1962) - Addenda No. EA - 2 (Feb. 1965), FORE, A Computational Program for the Analysis of Fast Reactor Excursions, by P. Greebler, and others.

15. Sanathanan, C. K., Carter, J. C., and Brittan, R. O., Transient Temperature Distribution in Fast Reactor Fuels with Widely Varying Thermal Diffusivity, Proceedings of the Conference on Safety, Fuels, and Core Design in Large Fast Power Reactors, Argonne National Laboratory ANL-7120, p. 478, Oct. 11-19, 1965.

16. Belle, J. (ed.), Uranium Dioxide: Properties and Nuclear Applications, Naval Reactors, Division of Reactor Development, U. S. Atomic Energy Commission, July, 1961.

17. Feith, A. D., "The Thermal Conductivity of UO_2 up to 2500°C", J. of Nuclear Materials, v. 16, p. 231, 1965.

18. Zames, G., "Functional Analysis Applied to Nonlinear Feedback Systems", IEEE Trans. Circuit Theory, p. 392, Sept. 1963.

19. Schultz, M. A., Control of Nuclear Reactors and Power Plants, McGraw-Hill Book Co., 1961.

20. Hildebrand, F. B., Introduction to Numerical Analysis, McGraw-Hill Book Co., 1956.

21. Conte, S. D., Elementary Numerical Analysis, McGraw-Hill Book Co., 1965.

22. Carslaw, H. S. and Jaeger, J. C., Conduction of Heat in Solids, Oxford University Press, 1959.

23. Nomuro, T. and Deiters, R. M., "Improving the Analog Simulation of Partial Differential Equations by Hybrid Computation", Simulation, p. 73, Aug. 1968.

24. Howe, R. M. and Hsu, S. K., Preliminary Investigation of a Hybrid Method for Solving PDE, 1968 Fall Joint Computer Conference, Dec. 9-11, 1968.

25. Thalgott, F. W., Fast Reactor Safety: EBR-I, Proceedings of the 1957 Fast Reactor Information Meeting, Argonne National Laboratory, p. 68, Nov. 20-21, 1957.

26. Nordheim, L. W., The Doppler Coefficient, The Technology of Nuclear Reactor Safety (vol. 1, Reactor Physics and Control), The MIT Press, Massachusetts Institute of Technology, p. 222, 1964.

27. Froelich, R., and others, Calculation of Doppler Coefficients of Dilute Fast Reactors, Conference on Breeding, Economics, and Safety in Large Fast Power Reactors, Argonne National Laboratory, Oct. 7-10, 1963.

28. Benjamin, M., "Introductory Survey of Basic Design and Fuel-Element Considerations for Large, Fast Sodium - Cooled Reactors", Nuc. Sci. and Eng., v. 7, p. 399, May, 1968.

29. Vichnevetsky, R., "Analog/Hybrid Solution of Partial Differential Equations in the Nuclear Industry", Simulation, p. 269, Dec, 1968.

INITIAL DISTRIBUTION LIST

		No. Copies
1.	Defense Documentation Center Cameron Station Alexandria, Virginia 22314	20
2.	Library, Code 0212 Naval Postgraduate School Monterey, California 93940	2
3.	Defense Atomic Support Agency Department of Defense Washington, D. C. 20315	1
4.	Professor A. Gerba Department of Electrical Engineering Naval Postgraduate School Monterey, California 93940	2
5.	Commandant United States Coast Guard 1300 E. Street, N. W. Washington, D. C. 20591	1
6.	LCDR Charles L. Keller 560 N. Beville Avenue Indianapolis, Indiana 46201	2
7.	Mr. Robert L. Limes, Code 52 Ec Department of Electrical Engineering Naval Postgraduate School Monterey, California 93940	1
8.	Professor G. A. Rahe, Code 52 Ra Department of Electrical Engineering Naval Postgraduate School Monterey, California 93940	1

Unclassified

Security Classification

DOCUMENT CONTROL DATA - R & D

(Security classification of title, body of abstract and indexing annotation must be entered when the overall report is classified)

1. ORIGINATING ACTIVITY *(Corporate author)*

Naval Postgraduate School
Monterey, California 93940

2a. REPORT SECURITY CLASSIFICATION

Unclassified

2b. GROUP

3. REPORT TITLE

Simulation of a Liquid Metal Fast Breeder Reactor on a Hybrid Computer

4. DESCRIPTIVE NOTES *(Type of report and inclusive dates)*

Master's Thesis, June 1969

5. AUTHOR(S) *(First name, middle initial, last name)*

Charles L. Keller

6. REPORT DATE	7a. TOTAL NO. OF PAGES	7b. NO. OF REFS
June 1969	84	29

8a. CONTRACT OR GRANT NO.	9a. ORIGINATOR'S REPORT NUMBER(S)
b. PROJECT NO.	
c.	9b. OTHER REPORT NO(S) *(Any other numbers that may be assigned this report)*
d.	

10. DISTRIBUTION STATEMENT

Distribution of this document is unlimited.

11. SUPPLEMENTARY NOTES	12. SPONSORING MILITARY ACTIVITY
	Naval Postgraduate School Monterey, California 93940

13. ABSTRACT

A Liquid Metal Fast Breeder Reactor is simulated on a hybrid computer to study the transient behavior of the neutron density during a controlled reactivity input disturbance.

The nonlinear partial differential equations of heat flow are reduced by a discrete space-continuous time method to ordinary nonlinear differential equations which are readily solved on the analog computer. Use is made of time multiplexing of the analog circuitry in order to reduce the number of components. An open-loop iteration process is employed to solve the closed-loop feedback system.

Recently conducted research with the open-loop iteration method has demonstrated that a large number of iterations are required for convergence. An algorithm is developed which gives an improvement in the convergence rate for early values of time. For times greater than two seconds a stability problem with the converged solution was encountered and is discussed with some observations and comments.

Innovations are introduced in the simulation of the neutron kinetics equations and in the handling of the nonlinear thermal properties of the uranium oxide fuel.

DD FORM 1 NOV 65 1473 (PAGE 1)

S/N 0101-807-6811

Unclassified

Security Classification

A-31408

14 KEY WORDS	LINK A		LINK B		LINK C	
	ROLE	WT	ROLE	WT	ROLE	WT
Hybrid Computer Simulation						
Liquid Metal Fast Breeder Reactor						